2021-12

Species turnover underpins the effect of elevated CO2 on biofilm communities through early succession

Allen, RJ

10.1016/j.ecochg.2021.100017
Climate Change Ecology
Elsevier BV

Species turnover underpins the effect of elevated CO2 on biofilm communities through early succession

Ro J. Allen , Tina C. Summerfield , Ben P. Harvey , Sylvain Agostini , Samuel P.S. Rastrick , Jason M. Hall-Spencer , Linn J. Hoffmann

PII: S2666-9005(21)00017-4
DOI: https://doi.org/10.1016/j.ecochg.2021.100017
Reference: ECOCHG 100017

To appear in: *Climate Change Ecology*

Received date: 28 February 2021
Revised date: 30 June 2021
Accepted date: 12 July 2021

Please cite this article as: Ro J. Allen , Tina C. Summerfield , Ben P. Harvey , Sylvain Agostini , Samuel P.S. Rastrick , Jason M. Hall-Spencer , Linn J. Hoffmann , Species turnover underpins the effect of elevated CO2 on biofilm communities through early succession, *Climate Change Ecology* (2021), doi: https://doi.org/10.1016/j.ecochg.2021.100017

Highlights

- High CO_2 conditions profoundly affected biofilm community composition
- Species turnover explained differences in community composition
- Biofilm communities were more homogeneous under high CO_2 conditions
- Toxin producing and turf-forming algae were enriched under high CO_2 conditions

Species turnover underpins the effect of elevated CO_2 on biofilm communities through early succession

Ro J. Allen[1], Tina C. Summerfield[1], Ben P. Harvey[2], Sylvain Agostini[2], Samuel P. S. Rastrick[3], Jason M. Hall-Spencer[2,4], Linn J. Hoffmann[1]

[1]Department of Botany, University of Otago, Dunedin 9054, New Zealand

[2]Shimoda Marine Research Center, University of Tsukuba, 5-10-1 Shimoda, Shizuoka, 415-0025, Japan

[3]Institute of Marine Research, PO Box 1870 Nordnes, 5817 Bergen, Norway

[4]Marine Biology and Ecology Research Centre, University of Plymouth, Plymouth, PL4 8AA, UK

Running head: Biofilm responses to ocean acidification

Keywords: biofilm, microbial ecology, harmful algae, ocean acidification, succession, CO_2 seeps

Correspondence:

Linn J. Hoffmann, Department of Botany, University of Otago, Dunedin 9054. Email: linn.hoffmann@otago.ac.nz Phone: +6434797577

Data accessibility statement: Sequencing data used in this study are accessible through the European Nucleotide Archive (accession: PRJEB39326)

Authorship: RA, LH, TCS, BH, and SA conceived and designed the experiment. RA, BH, SA, SR, and JHS collected the data. RA performed the data analyses. RA wrote the first draft of the manuscript with LH and TCS, and all authors contributed substantially to revisions.

Abstract

Biofilms harbour a wealth of microbial diversity and fulfil key functions in coastal marine ecosystems. Elevated carbon dioxide (CO_2) conditions affect the structure and function of biofilm communities, yet the ecological patterns that underpin these effects remain unknown. We used high-throughput sequencing of the 16S and 18S rRNA genes to investigate the effect of elevated CO_2 on the early successional stages of prokaryotic and eukaryotic biofilms at a CO_2 seep system off Shikine Island, Japan. Elevated CO_2 profoundly affected biofilm community composition throughout the early stages of succession, leading to greater compositional homogeneity between replicates and the proliferation of the potentially harmful algae *Prymnesium* sp. and *Biddulphia biddulphiana*. Species turnover was the main driver of differences between communities in reference and high CO_2 conditions, rather than differences in richness or evenness. Our study indicates that species turnover is the primary ecological pattern that underpins the effect of elevated CO_2 on both prokaryotic and eukaryotic components of biofilm communities, indicating that elevated CO_2 conditions represent a distinct niche selecting for a distinct cohort of organisms without the loss of species richness.

1 | Introduction

Biofilms are complex aggregates of microbes on solid surfaces in aquatic environments (Costerton *et al.* 1995). They are the dominant mode of microbial life on Earth by cell abundance (Flemming and Wuertz 2019), and harbour a wealth of prokaryotic and eukaryotic diversity (Sanli *et al.* 2015; Flemming *et al.* 2016). Biofilm microbes live within a matrix of extracellular polymeric substances (EPS) which facilitate bioadhesion (Flemming and Wingender 2010), and act as a platform for the extracellular breakdown of organic compounds (Pohlon, Marxsen and Küsel 2010), intercellular communication (De Kievit 2009), and the storage of excess carbon as polysaccharides (Flemming and Wingender 2010). Biofilms are basal components of coastal marine ecosystems, where they are a food-source for benthic grazers (Thompson, Norton and Hawkins 2004) and the primary settlement substratum for many ecosystem engineers, including scleractinian corals (Tran and Hadfield 2011; Espinel-Velasco *et al.* 2018).

Ocean acidification, due to rising atmospheric carbon dioxide (CO_2) concentrations, has decreased mean surface ocean pH by 0.1 units since the pre-industrial era, and is projected to drive a further decrease of 0.3 pH units by the end of the century under the Intergovernmental Panel on Climate Change 'business-as-usual' emissions scenario (RCP 8.5) (Hoegh-Guldberg *et al.* 2014). Increased CO_2 concentrations can enhance microalgal growth rates by reducing the energetic cost of photosynthesis, but can also impact other physiological processes including intracellular pH homeostasis and calcification (Mackey *et al.* 2015). By acting as both a stressor and a resource, ocean acidification can alter competitive interactions and the community composition of marine organisms, leading to substantial reshaping of ecosystems (Connell *et al.* 2018).

Laboratory studies indicate that ocean acidification has both direct and indirect effects on biofilm communities. For example, laboratory experiments in flow-through aquaria

demonstrate that high CO_2 conditions alter biofilm community composition when biofilms are isolated from the wider ecological community (i.e. grazers and other benthic organisms; Witt *et al.* 2011a; Nelson *et al.* 2020; Espinel-Velasco *et al.* 2021), while laboratory experiments including grazing gastropods indicate that high CO_2 conditions can indirectly affect biofilm communities by reducing grazing rates (Russell *et al.* 2013). Since biofilms play a critical role in benthic ecosystems, studies in natural environmental settings are needed to gain a holistic understanding of how biofilm ecology will be impacted by future conditions (Russell *et al.* 2013). At volcanic seeps, CO_2 percolates through the seafloor and dissolves in seawater creating areas of localised acidification comparable to conditions projected by the end of the century (Hall-Spencer *et al.* 2008; Agostini *et al.* 2015). These systems facilitate investigations into the ecosystem-level effects of ocean acidification in a setting of chronic exposure and natural realism (Hall-Spencer *et al.* 2008; Andersson *et al.* 2015).

Studies at CO_2 seeps have demonstrated that ocean acidification can significantly alter the composition of prokaryotic biofilm communities on natural and artificial substrata (Lidbury *et al.* 2012; Kerfahi *et al.* 2014; Taylor *et al.* 2014). Studies of eukaryotic biofilm communities at CO_2 seeps have reported altered community composition, increased diatom abundance, and higher relative abundance of large chain-forming diatom species (Lidbury *et al.* 2012; Johnson *et al.* 2013, 2015). While these studies demonstrate that ocean acidification can affect the structure of biofilm communities, ecological patterns underpinning biofilm community responses to ocean acidification are currently unknown.

Differences in community composition through space or time can emerge from two fundamental patterns called ‘turnover’ and ‘nestedness’, these two patterns are not mutually exclusive (Baselga 2010). ‘Turnover’ is the replacement of species in one community with different species in another community. ‘Nestedness’ is when species occurring in one community are a subset of species occurring in another community (Fig. S1). In the context

of this study, turnover as the dominant ecological pattern would suggest that conditions at reference and high CO_2 sites represent distinct niches, selecting for distinct cohorts of organisms while maintaining richness. In contrast nestedness as the dominant ecological pattern would suggest that the cohort of organisms under high CO_2 conditions consisted of a CO_2-tolerant subcomposition of organisms present under reference conditions. Unravelling these distinct patterns provides deeper insights into the nature of differences between communities (Baselga 2010; Baselga and Orme 2012).

Here, we investigated the effects of ocean acidification on the composition, diversity, and early successional dynamics of biofilm communities over 21 days at a CO_2 seep system off Shikine Island, Japan. We used high-throughput amplicon sequencing of the 16S rRNA gene (Caporaso *et al.* 2011; Apprill *et al.* 2015) and 18S rRNA gene (Stoeck *et al.* 2010; Massana *et al.* 2015) to characterise prokaryotic and eukaryotic components of biofilm communities, respectively. We hypothesised that elevated CO_2 conditions would lead to distinct eukaryotic and prokaryotic biofilm community composition driven primarily by turnover, due to the duality of CO_2 as both a stressor and a resource. These data provide the most detailed assessment of biofilm community composition at CO_2 seeps to date, and shed new light on the ecological patterns that underpin the responses of biofilms to near-future ocean acidification.

2 | Materials and methods

2.1 | Study site and sampling

Shikine Island (34.325 ºN, 139.210 ºE) is a volcanic island approximately 50 km south east of Shimoda, Japan. It is at a temperate latitude but is influenced by the warm Kuroshio current and so the coastal waters of this island host a diverse range of tropical and temperate organisms including scleractinian corals and canopy-forming macroalgae (Agostini *et al.*

2018). The island has a well described CO_2 seep system in Mikawa Bay where ~98% CO_2 gas percolates through the seafloor creating areas of localised acidification (Agostini *et al.* 2015; Harvey *et al.* 2018), and an adjacent bay used as a reference site that is unaffected by the CO_2 seep system (Fig. 1). The two sites used in this study had very similar temperature, salinity, total alkalinity, nutrients, depth, currents, and dissolved oxygen conditions (Agostini *et al.* 2015, 2018; Harvey *et al.* 2019) (Fig. S2). Benthic communities significantly differ between reference and high CO_2 sites (Agostini *et al.* 2018), while planktonic bacterial communities do not significantly differ between sites (Kerfahi *et al.* 2020).

The carbonate chemistry of the two sites was previously published in Harvey *et al.* (2021) where the experimental period encompassed the present study. Briefly, durafet pH sensors (Seafet, Sea-Bird Scientific, Canada) were deployed at 5 m depth at the reference site and high CO_2 site to record ambient pH_{total} and temperature at 15-minute intervals. Salinity was measured concurrently using Hobo conductivity loggers (U24-002-C), and discrete samples for total alkalinity were collected throughout the study period from 5-6 m depth, with total alkalinity measured using an auto-titrator (916 Ti-Touch, Metrohm). Carbonate chemistry parameters were calculated using CO2SYS (Pierrot et al. 2006), with pH_{total}, total alkalinity, temperature, and salinity as input variables (Table 1).

To survey the early-succession of biofilm communities under reference and high CO_2 conditions, we deployed nine rigs at a depth of 5-7 m within each site between 30th May and 20th June 2017. Each rig held four 5 cm x 10 cm transparent acrylic slides, 10 cm above the benthos, situated with the widest part of the slide facing the surface. Rigs were not designed to exclude grazers. One slide was collected from each rig at 5, 10, 15 and 21 days after deployment, a total of nine replicates per site and time point. The experimental period of 21 days was sufficient for visible biofilms to fully colonise the slides (Fig. S7), and aligned with

previous experimental periods used in ocean acidification studies (e.g. Witt *et al.* 2011; Johnson *et al.* 2013).

After collection, a 30 cm^2 section of biofilm was removed from the upper surface of each slide using a sterile razorblade and transferred into a 2 ml cryovial. Cryovials were immediately frozen in liquid nitrogen prior to DNA extraction. The remaining 20 cm^2 section of biofilm was removed from the upper surface of each slide using a sterile razorblade and transferred to a 2 ml microfuge tube for chlorophyll *a* analysis. Chlorophyll *a* was extracted from biofilm samples in 1 ml of 96% ethanol over a 24-hour period at -20°C. Following this incubation period, each microfuge tube was centrifuged at 5,000 x *g* for 5 minutes to remove particulate matter. The supernatant was used to determine chlorophyll *a* concentration following spectrophotometric methods described in Jeffrey and Humphrey (1975) using a UV-1280 UV-VIS Spectrophotometer (Shimadzu Corporation, Kyoto, Japan).

2.2 | Amplicon sequencing

Genomic DNA was extracted from each biofilm sample using the Qiagen DNEasy Plant Mini Kit (Qiagen, Valencia, CA, USA) according to the manufacturer's instructions. A two-round PCR protocol was used to generate paired-end Illumina libraries for 16S and 18S rRNA genes, respectively. In the first round, the V4 region of the 16S rRNA gene was amplified using the 515F (5' GTGYCAGCMGCCGCGGTAA) and 806R (5' GGACTACNVGGGTWTCTAAT) primers (Apprill *et al.* 2015; Parada, Needham and Fuhrman 2016), and the V4 region of the 18S rRNA gene was amplified using the TAReuk454FWD1 (5'CCAGCASCYGCGGTAATTCC) and TAReukREV3 (5' ACTTTCGTTCTTGATYRA) primers (Stoeck *et al.* 2010). Both sets of primers were modified to allow the downstream attachment of Illumina TruSeq sequencing adapters and indexes (Illumina, San Diego, CA, USA; Griffith *et al.* 2017). Triplicate 25 µl PCR mixtures

were prepared for each DNA sample using the HiFi Hotstart PCR kit (KAPA Biosystems, Boston, MA, USA). The PCR thermocycler program for the 16S rRNA gene had an initial denaturation step at 95°C for 120 s, followed by 25 cycles of 98°C for 20 s, 60°C for 30 s, and 72°C for 30 s, with a final extension period of 60 s at 72°C. The PCR thermocycler program for the 18S rRNA gene was adapted from Massana et al. (2015) and had an initial denaturation step at 95°C for 30 s, followed by 10 cycles of 95°C for 30 s, 53°C for 30 s, and 72°C for 30 s, followed by 15 cycles of 95°C for 30 s, 48 °C for 30 s, and 72°C for 30 s, with a final extension period of 300 s at 72°C. Resulting triplicate PCR products from each sample were pooled and purified using the Mag-bind TotalPure NGS kit (OMEGA Bio-tek, Norcross, GA, USA). The DNA concentration of the purified PCR products was quantified using the Qubit dsDNA High Sensitivity Assay (Thermo Fisher Scientific, Waltham, MA, USA), and purified PCR products were diluted to 1 ng μl^{-1}.

A second round of PCR was performed to attach Illumina TruSeq sequence adapters and indexes. Each PCR mixture was prepared as described above and contained 1 µl of diluted first round PCR products. The PCR thermocycler program had an initial denaturation step at 95°C for 120 s, followed by 10 cycles of 98°C for 20 s, 60°C for 20 s, and 72°C for 20 s, with a final extension period of 60 s at 72°C. Second round PCR products were purified, quantified, and pooled to generate libraries for the 16S rRNA gene and 18S rRNA gene. Pooled libraries were sequenced on the Illumina MiSeq platform (Illumina, San Diego, CA, USA) using the V2 (2 x 250 bp) and V3 (2 x 300 bp) reagent kits for the 16S rRNA gene and 18S rRNA gene, respectively. Sequence data are available through the European Nucleotide Archive (accession: PRJEB39326).

16S rRNA gene and 18S rRNA gene sequences were processed according to the Bioconductor workflow for microbiome data analysis (Callahan *et al.* 2016b). Primers were trimmed from forward and reverse reads at positions 20 and 18, respectively, and low-quality

sequences were truncated from forward and reverse reads at positions 200 and 170, respectively for 16S rRNA gene sequences using the *filterAndTrim* function in the R package 'dada2' (Callahan *et al.* 2016a). Primers were trimmed from forward and reverse 18S rRNA gene sequences at positions 20 and 18, respectively, and low-quality sequences were truncated from forward and reverse reads at positions 300 and 275, respectively. For both 16S and 18S rRNA gene sequences, a maximum of 2 expected errors (maxEE) were allowed. Following trimming, the DADA2 method (Callahan *et al.* 2016a) was used to infer amplicon sequence variants (ASVs) at the single nucleotide resolution. Chimeric sequences were removed, and taxonomy was assigned using the RDP Naïve Bayesian classifier (Wang *et al.* 2007) against the SILVA release 132 database (Quast *et al.* 2013) and PR2 version 4.10.0 database (Guillou *et al.* 2013) for 16S rRNA gene and 18S rRNA gene ASVs, respectively. 16S rRNA gene ASVs which were not classified as *Bacteria* or *Archaea*, or were classified as chloroplasts or mitochondria, were filtered prior to downstream analysis. Similarly, 18S rRNA gene ASVs were filtered to remove metazoan sequences, which were not a target of this study as the sampling design was not appropriate to representatively sample metazoans, and metazoan sequences have the potential to dominate sample read counts. The 20 most abundant ASVs in both 16S rRNA gene and 18S rRNA gene datasets were further classified through a BLASTn search of the NCBI database excluding uncultured and environmental sample sequences (accessed May 2020; Table S1). Resulting ASV tables, taxonomy tables, and corresponding environmental metadata were assembled as a phyloseq object (McMurdie and Holmes 2013) for 16S rRNA gene and 18S rRNA gene ASVs, respectively. Sequence reads were then randomly subsampled to an even depth (16S rRNA gene: 15,893, 18S rRNA gene: 11,689 reads), and as a result of this process three 16S rRNA gene samples (high CO_2: R10D5, R15D5, R15D15) and three 18S rRNA gene samples (reference: R6D21; high CO_2: R10D5, R15D5) were excluded due to insufficient sequencing depth. Rarefaction curves for

16S rRNA gene and 18S rRNA gene reads indicate that rarefaction depth was sufficient to capture a representative proportion of ASV richness in each sample (Fig. S3).

2.3 | Statistical analyses

Jaccard dissimilarity, a measure of dissimilarity based on the binary presence or absence of species between samples, was used to quantify pairwise dissimilarity between biofilm communities using rarefied read counts as an input. Jaccard dissimilarity can be decomposed to partition dissimilarity between turnover and nestedness components (Baselga and Orme 2012; Fig. S1). Pairwise dissimilarity matrices of Jaccard dissimilarity, the turnover component of Jaccard dissimilarity (hereafter turnover), and the nestedness component of Jaccard dissimilarity (hereafter nestedness), were calculated using the *beta.pair* function in the R package 'betapart' (Baselga and Orme 2012). These dissimilarity matrices were then used as an input for PERMANOVA (Anderson 2001), implemented through the *adonis* function in the R package 'vegan' (Oksanen *et al.* 2016), to test the effect of CO_2 condition (reference and high CO_2), time point (day 5, day 10, day 15, and day 21), and the interaction between CO_2 condition and time point, on both prokaryotic and eukaryotic community composition. Pairwise comparisons were then performed between reference and high CO_2 conditions at each time point, and between each pair of time points at reference and high CO_2 conditions, respectively.

Homogeneity of multivariate dispersion of prokaryotic and eukaryotic biofilm communities between CO_2 conditions and time points, based on Jaccard dissimilarity, were obtained and tested permutationally using the *betadisper* function in the R package 'vegan' (Anderson, Ellingsen and McArdle 2006). Homogeneity of multivariate dispersions are based on distance-to-centroid values, which are calculated as the distance of an individual community (sample) to the centroid of the group to which the community belongs (e.g. high CO_2, day 5)

and represents a measure of compositional variability. Homogeneity of multivariate dispersions is also an important analysis to inform the interpretations of PERMANOVA results, as significant differences in community composition identified by PERMANOVA can emerge both from differences in centroid position and from differences in homogeneity of multivariate dispersion. Pairwise tests were performed between each pair of time points under reference and high CO_2 conditions, and between reference and high CO_2 conditions at each time point, respectively.

Both PERMANOVA and homogeneity of multivariate dispersions analyses were repeated using Bray-Curtis dissimilarity, an alternative metric to Jaccard dissimilarity based on abundance rather than presence or absence, for comparison. This comparison allows the effect of both the presence and absence of different taxa, and changes in relative abundance of taxa, in driving trends in beta-diversity to be better understood.

The richness and evenness of prokaryotic and eukaryotic biofilm communities were quantified using the Chao1 index (Chao 1984) and Pielou's evenness (Pielou 1966), respectively. A two-way ANOVA with Tukey's HSD was then used to test the effects of CO_2 condition and time point on eukaryotic and prokaryotic biofilm community richness and evenness.

Finally, the effect of CO_2 condition and time point on biofilm chlorophyll *a* concentration was compared using a two-way ANOVA with Tukey's HSD, to investigate differences in the standing stock of photosynthetic organisms in total biofilm communities. All statistical analyses were performed in the R environment (R Core Team 2013).

3 | Results

3.1 | Community composition

Prokaryotic and eukaryotic community composition were significantly affected by both CO_2 condition and time point, with a significant interaction between these factors (Table 2; Fig. 2). Pairwise analysis revealed significant differences in prokaryotic and eukaryotic community composition between reference and high CO_2 conditions at all time points, and between each pair of time points under both reference and high CO_2 conditions (Table 2). Turnover displayed highly similar patterns to Jaccard dissimilarity, as both CO_2 condition and time point affected turnover with a significant interaction between these factors (Table 2; Fig. 2). In contrast, CO_2 condition and time point did not affect nestedness (Table 2; Fig. 2).

Analysis of homogeneity of multivariate dispersions showed that the compositional variability of prokaryotic and eukaryotic biofilm communities significantly differed between CO_2 conditions (Betadisper; prokaryotes: $F = 6.26$, $p < 0.05$; eukaryotes: $F = 6.83$, $p < 0.05$; Fig. 3). In prokaryotic communities, compositional variability was lower under high CO_2 conditions compared with reference conditions at day 5, day 15, and day 21 (all $p < 0.01$). In eukaryotic communities, compositional variability was lower under high CO_2 conditions compared with reference conditions at day 5 and day 21 (both $p < 0.01$). While homogeneity of multivariate dispersions significantly differed between reference and high CO_2 conditions, inspection of NMDS ordinations (Fig 2) shows clear differences in centroid position between reference and high CO_2 conditions indicating that significant PERMANOVA results mentioned above do not exclusively results from differences in homogeneity of multivariate dispersions. Repeating PERMANOVA and homogeneity of multivariate dispersion analyses based on Bray-Curtis dissimilarity, rather than Jaccard dissimilarity, yielded highly similar results (Table S1, Fig. S4).

At the Phylum level (further classified by Class for *Proteobacteria*), prokaryotic communities were dominated by *Alphaproteobacteria* (reference: 39.7% ± 18.9 (mean ± SD), high CO_2: 40.7% ± 8.7) and *Bacteroidetes* (reference: 38.7% ± 12.4, high CO_2: 36.0% ± 7.7) under both

reference and high CO_2 conditions across all time points during the study (Fig. 4). *Gammaproteobacteria* were a consistent feature of prokaryotic communities under high CO_2 conditions (16.6% ± 4.4) but represented a smaller and more variable component of communities under reference conditions (12.6% ± 6.7). Similarly, *Verrucomicrobia* were a variable component of prokaryotic communities under reference conditions (6.1% ± 7.0), but were a smaller and less variable component of prokaryotic communities under high CO_2 conditions (3.2% ± 1.8). Profiles of prokaryotic community composition at the Order level are included in the supplementary information (Fig. S5). Trends in prokaryotic biofilm community composition amongst abundant ASVs were subtle under reference conditions, though *Loktanella* sp. asv_8, *Rhodobacteraceae* sp. asv_6, and *Rubritalea* sp. asv_14 sporadically dominated samples (Fig. 4). In contrast, under high CO_2 conditions, prokaryotic communities displayed clear structuring through time amongst the most abundant ASVs. Under high CO_2 conditions, *Rhodobacteraceae* sp. asv_6 (4.1% ± 1.0), *Rhodobacteraceae* sp. asv_27 (3.6% ± 0.8), *Thalassobius aestuarii* asv_35 (3.3% ± 0.7), and *Rhodobacteraceae* sp. asv_5 (2.9% ± 0.7) had the greatest relative abundance at day 5. By day 21 *Fabivirga thermotolerans* asv_9 (4.3% ± 2.3), *Tateyamaria* sp. asv_17 (4.4% ± 0.8), *Alteromonas macleodii* asv_21 (4.1% ± 2.4), and *Kordia* sp. asv_13 (3.9% ± 1.4) had the greatest relative abundance.

At the Division level, other *Stramenopiles*, which included *Oomycota* and *Labyrinthulea*, represented a substantial but highly variable component of eukaryotic communities under reference conditions (15.0% ± 15.4; Fig. 5) but not under high CO_2 conditions (4.5% ± 4.3). Similarly, *Ciliophora* were a greater component of eukaryotic communities under reference conditions (6.3% ± 4.9) than under high CO_2 conditions (1.8% ± 1.3). In contrast, *Rhodophyta* represented a greater proportion of eukaryotic communities under the high CO_2 conditions (14.1% ± 9.9) compared to under reference conditions (3.6% ±

3.3). At day 5, *Chlorophyta* were a substantial component of eukaryotic communities under both reference and high CO_2 conditions (reference: 13.8% ± 5.7, high CO_2: 24.9% ± 5.8), but the relative abundance of *Chlorophyta* was lower at other time points (reference: 2.3% ± 2.0, high CO_2: 0.9% ± 0.64). From day 10 onwards, *Haptophyta* had a greater relative abundance under high CO_2 conditions (34.9% ± 13.5) than under reference conditions (16.0% ± 10.4). Profiles of eukaryotic community composition at the Order level are included in the supplementary information (Fig. S6). Generally, division-level trends in eukaryotic community composition were driven by a small number of highly abundant ASVs (Fig. 5). At day 5, reference condition communities were dominated by *Ectocarpus* sp. asv_3 (22.4% ± 14.8) and *Anisolpidium rosenvingei* asv_6 (22.4% ± 20.1). Under high CO_2 conditions, *Phaeophyceaea* sp. asv_2 (15.2% ± 5.6) and *Phaeophyceaea* sp. asv_12 (16.7% ± 4.0) were the most abundant taxa, whilst *Ectocarpus* sp. asv_3 (1.5% ± 0.4) and *Anisolpidium rosenvingei* asv_6 (0.2% ± 0.4) were rare or absent. From day 10 onwards, *Prymnesium sp*. asv_1 (14.3% ± 9.9) and *Phaeophyceaea* sp. asv_2 (22.0% ± 20.7) had the greatest relative abundance under reference conditions, whilst *Prymnesium* sp. asv_1 (30.8% ± 12.1) dominated under high CO_2 conditions and *Biddulphia biddulphiana* asv_11 (3.5% ± 9.2%) appeared sporadically, colonising 26 of 34 slides with a maximum relative abundance of 38.9%.

3.2 | Richness and evenness

Prokaryotic richness (Chao1 index) was significantly affected by time point ($F_{3,61}$ = 9.953, p < 0.001) but not CO_2 condition ($F_{1,61}$ = 0.027, p > 0.05), with no significant interaction between these factors ($F_{3,61}$ = 0.623, p > 0.05; Fig. S8a). Prokaryotic richness was lower at day 5 than at day 10 under reference conditions (p < 0.05), and was higher at day 10 than day 21 under both reference and high CO_2 conditions (p < 0.05) but did not differ between any

other time points (all $p > 0.05$). Prokaryotic biofilm community evenness (Pielou's evenness) was significantly affected by CO_2 condition ($F_{1,61} = 5.153$, $p < 0.05$) and time point ($F_{3,61} = 3.995$, $p > 0.05$), with no significant interaction between these factors ($F_{3,61} = 0.058$, $p > 0.05$; Fig. S8c). However, pairwise comparisons revealed no significant difference between reference and high CO_2 conditions at any time point (all $p > 0.05$; Fig. S8c).

Eukaryotic richness was significantly affected by time point ($F_{3,61} = 67.460$, $p < 0.001$), but not CO_2 condition ($F_{1,61} = 1.598$, $p > 0.05$), with a significant interaction present between these factors ($F_{3,61} = 4.883$, $p < 0.05$; Fig. S8b). Pairwise comparisons revealed that eukaryotic richness under high CO_2 conditions was greater at day 5 than day 15 and day 21 (both $p < 0.05$), but did not differ between any other time points under either reference or high CO_2 conditions (all $p > 0.05$). Eukaryotic evenness was significantly affected by time point ($F_{3,61} = 3.894$, $p < 0.05$) but not CO_2 condition ($F_{1,61} = 0.079$, $p > 0.05$) with a significant interaction between these factors ($F_{3,61} = 3.772$, $p < 0.05$). However, pairwise comparisons revealed no significant differences between time points under either reference or high CO_2 conditions (all $p > 0.05$; Fig S8d).

3.3 | Chlorophyll *a*

Chlorophyll *a* concentration was significantly affected by time point ($F_{3,64} = 18.67$, $p < 0.001$), but not CO_2 condition ($F_{1,64} = 0.18$, $p > 0.05$), and there was no significant interaction between these factors ($F_{3,64} = 0.76$, $p > 0.05$). Chlorophyll *a* concentrations under both the reference and high CO_2 conditions were greater at day 10, day 15, and day 21, when compared with day 5 (all $p < 0.001$), but did not significantly differ between any other time points (Fig. S9).

4 | Discussion

4.1 | Community composition

Prokaryotic and eukaryotic community composition under high CO_2 conditions differed from reference conditions at all time points in this study, in line with findings from Mediterranean CO_2 seeps on both natural (Lidbury *et al.* 2012; Johnson *et al.* 2013) and artificial substrata (Kerfahi *et al.* 2014; Taylor *et al.* 2014; Johnson *et al.* 2015). By partitioning Jaccard dissimilarity into turnover and nestedness components, we demonstrate that species turnover rather than nestedness is the primary driver of differences in community composition between reference and high CO_2 conditions for both prokaryotes and eukaryotes (Fig. 2). These data suggest that environmental conditions at reference and high CO_2 sites represent distinct niches, which select for distinct cohorts of prokaryotic and eukaryotic microbes. Nestedness would be the dominant ecological pattern if biofilm communities developing under high CO_2 conditions consisted of a CO_2-tolerant subset of species present under reference conditions. However, this was not the case, in-line with the notion that high CO_2 conditions can act as both a stressor and a resource for photosynthetic organisms in coastal marine ecosystems (Connell *et al.* 2018).

Similar differences in prokaryotic and eukaryotic community composition between reference and high CO_2 sites emerged when repeating these analyses based on Bray-Curtis dissimilarity, rather than Jaccard dissimilarity. This indicates that differences in the relative abundance of organisms, in addition to the presence and absence of organisms, contribute to difference in community composition between sites and timepoints (Table S1, Fig. S4). It should further be noted that differences in benthic community assemblages at each site (including reduced hard coral cover, reduced crustose coralline algae cover, reduced calcifying fauna, and increased fleshy algae cover at high CO_2 sites; Agostini *et al.* 2018) may result in differences in recruitment pools from which biofilms assemble at each site, and

consequently this could be a mechanism which contributes to differences in biofilm community composition observed in this study.

Both prokaryotic and eukaryotic communities displayed greater homogeneity under high CO_2 conditions (Fig. 3). Greater homogeneity in community composition under high CO_2 conditions has previously been observed in macroscopic biofouling (Brown, Therriault and Harley 2016; Brown *et al.* 2018; Brown, Bernhardt and Harley 2020) and algal communities (Porzio, Buia and Hall-Spencer 2011; Kroeker, Micheli and Gambi 2012). Olden *et al.* (2004) highlight that homogenisation of biotic communities can result in an increased vulnerability of ecosystems to environmental changes (e.g. marine heatwaves), decreased resilience to disturbance (e.g. severe weather), and altered ecosystem function (e.g. biogeochemical cycling) primarily as a result of reduced functional diversity. Consequently, it is pertinent to establish whether the increased homogenisation of biofilm, biofouling, and algal communities under high CO_2 conditions can be generalised broadly to coastal marine ecosystems.

4.2 | Succession

Prokaryotic and eukaryotic communities differed significantly between each successive time point in this study, driven primarily by species turnover (Fig. 2). Kroeker et al. (2012) observed that benthic communities colonising settlement tiles under ambient and high CO_2 conditions developed similarly through early successional stages, only diverging after 3.5 months as fleshy algae outcompeted calcareous taxa. In our study, the composition of both prokaryotic and eukaryotic communities was distinct between reference and high CO_2 conditions at day 5, before chlorophyll *a* concentration had peaked (Fig. S9), indicating that community composition differed before slides were completely colonised. These data suggest that high CO_2 conditions impact biofilm community composition through early stages of biofilm development before competition for space becomes a factor.

We also note that 18S rRNA gene sequences belonging to the Class *Phaeophyceaea* and Genus *Ectocarpus* (a member of the *Phaeophyceaea*) appear to be more prevalent and abundant under reference conditions (Fig. 5a, asv_3, asv_2) suggesting that high CO_2 conditions may affect macroalgal recruitment and succession as demonstrated in previous studies (Porzio, Buia and Hall-Spencer 2011; Porzio, Garrard and Buia 2013; Harvey *et al.* 2021b). However, the sampling period used in this study was not sufficient for the investigation of macroalgal community succession.

4.3 | Richness and evenness

The richness and evenness of prokaryotic communities did not significantly differ between reference and high CO_2 sites at any time point (Fig. S8a, c). Previous CO_2 seep studies have reported contrasting effects of ocean acidification on prokaryotic diversity. Hassenrück et al. (2017) reported no effect of high CO_2 on prokaryotic richness over 13-months of biofilm development. Kerfahi et al. (2014) showed that prokaryotic diversity in epipelic communities was greater under high CO_2 conditions. Similarly, Lidbury et al. (2012) found that prokaryotic diversity was enhanced under high CO_2 conditions, but that these effects were modulated by light conditions, and Kerfahi et al. (2020) found that prokaryotic diversity was greater under high CO_2 conditions in intertidal epilithic biofilms. In contrast, Taylor et al. (2014) reported that prokaryotic diversity in epilithic biofilms was lower under high CO_2 conditions.

Eukaryotic community richness was significantly enhanced under high CO_2 conditions at day 5, but at no other time point (Fig. S8b). Eukaryotic richness did not differ between conditions beyond day 5, aligning with the findings of previous CO_2 seep studies of eukaryotic biofilm communities (Lidbury *et al.* 2012) but contrasting with those focussing exclusively on photosynthetic eukaryotes (Johnson *et al.* 2013, 2015). Eukaryotic evenness

did not significantly differ between reference and high CO_2 conditions at any time point (Fig S8d), in line with the findings of previous investigations of eukaryotic biofilm communities (Lidbury *et al.* 2012) but contrasting with studies of photosynthetic eukaryotes which show the dominance of a smaller cohort of taxa under high CO_2 conditions (Johnson *et al.* 2013, 2015).

Our study provides greater taxonomic resolution and depth than previous reports as a result of methodological differences, yet it is apparent that the effects of ocean acidification on biofilm richness and evenness can differ profoundly between substrates, studies, and regions. Moreover, previous reports indicate that factors other than the CO_2 can have a substantially greater effect on prokaryotic diversity over long time periods, potentially masking the comparatively subtle effects of CO_2 (Hassenrück *et al.* 2017). Taken together, these data suggest the effects of elevated CO_2 on biofilm community richness and evenness are dependent on complex interactions with other environmental variables, and defining general rules remain elusive.

4.4 | Harmful algae

From day 10 onwards, eukaryotic communities under high CO_2 conditions were dominated by *Prymnesium* sp. (Fig. 5a; Fig. 6a), a genus of mixotrophic golden algae responsible for the production of prymnesins and other compounds with toxic and allelopathic effects (Manning and La Claire 2010; Seoane, Riobó and Franco 2017). The species-level classification of *Prymnesium* sp. ASVs in this study could not be distinguished based on 18S rRNA gene V4 region amplicons. However, toxicity is ubiquitous across all strains of the genus examined to date (Seoane, Riobó and Franco 2017). *Prymneisum pavrum* specifically can form harmful blooms resulting in large-scale fish kills with significant socioeconomic implications (Roelke *et al.* 2016). Furthermore, *Prymnesium pavrum* consume

microbes affected by their toxins (Roelke *et al.* 2016), whilst the allelopathic nature of prymnesins can reduce grazing pressure and suppress competition from other microalgae (Fistarol, Legrand and Granéli 2003; Roelke *et al.* 2016). These factors simultaneously increase the fitness of *Prymnesium pavrum* and decrease the fitness of competitors (Roelke *et al.* 2016). Prosser et al. (2012) found that low pH conditions suppress bloom formation in *Prymnesium parvum*, but they manipulated pH through sulfuric acid addition rather than CO_2 addition, and consequently their study is not directly comparable. We suggest that *Prymnesium* sp. may be able to capitalise on the increased availability of dissolved inorganic carbon under high CO_2 conditions, which increases toxin production in other microalgae (Hall-Spencer and Allen 2015), allowing them to dominate the eukaryotic component of biofilms. Riebesell et al. (2018) have also shown that some toxic microalgae are able to capitalise on projected near-future CO_2 concentrations at the ecosystem level.

The large chain-forming diatom *Biddulphia biddulphiana* sporadically colonised slides under high CO_2 conditions (Fig. 5a; Fig. 6b). These diatoms can form thick mats of turf-like algae that overgrow corals and macroalgae, smothering the benthos (Galland and Pennebaker 2012; Harvey *et al.* 2019). However, little is known about the environmental conditions which induce such events (Galland and Pennebaker 2012). Our findings demonstrate that these diatoms are able to rapidly colonise available substrate under high CO_2 conditions, suggesting that the availability of inorganic carbon may be an important environmental factor in the formation of *Biddulphia biddulphiana* blooms. Indeed, under high CO_2 conditions around Shikine Island, *Biddulphia biddulphiana* blooms have been shown to overgrow benthic habitats driving the simplification of these coastal ecosystems (Harvey *et al.* 2019, 2021a, 2021b). *Biddulphia biddulphiana* blooms were present near the high CO_2 site during the experimental period, but not where slides were deployed. These data

add to growing body of evidence indicating that large chain-forming diatom species may benefit from high CO_2 conditions (Johnson *et al.* 2013, 2015).

4.5 | Implications for ecosystem shifts

Differences in the composition of prokaryotic and eukaryotic biofilm communities between reference and high CO_2 sites may affect the recruitment of invertebrates and habitat-forming organisms, which has previously been shown to be impacted by ocean acidification (Cigliano *et al.* 2010; Fabricius *et al.* 2015; Allen *et al.* 2016). Espinel-Velasco et al. (2018) highlight the importance of biofilm community composition in modulating the effects of ocean acidification on invertebrate recruitment. Nelson *et al.* (2020) showed altered settlement of serpulid worms on biofilms established under elevated CO_2 conditions, indicating a mechanistic role of altered biofilm community composition. Moreover, Fabricius et al. (2017) found that scleractinian coral recruitment was more severely affected by pCO_2-associated shifts in substratum composition than by the direct effects of seawater chemistry. Our findings demonstrate clear shifts in biofilm community composition under high CO_2 conditions, which may have consequences spanning multiple trophic levels.

Harvey *et al.* (2021b) investigated benthic community assembly over a 12-month period at the same reference and high CO_2 sites used in this study. They found reduced recruitment of macrophyte algae, and increased recruitment of microalgae and turf-forming algae at under high CO_2 conditions. Reciprocal transplants of communities preestablished under high CO_2 conditions to the reference site were indicative of a high degree of resilience in benthic community composition, as transplanted communities became indistinguishable from those established under reference CO_2 conditions over a 6-month period following transplantation. This suggests that while biofilm community composition may play an important role in the early stages of benthic community development, they are unlikely to be

responsible for the fixation (or 'locking in') of simplified turf algal communities characteristic of high CO_2 sites (Harvey *et al.* 2021a). Nonetheless, shifts in biofilm community composition and consequent effects on the recruitment of invertebrates and habitat-forming organisms may contribute to the restructuring of coastal marine environments and associated impacts on ecosystem services observed under high CO_2 conditions at CO_2 seeps globally (Hall-Spencer *et al.* 2008; Fabricius *et al.* 2011; Agostini *et al.* 2018; Hall-Spencer and Harvey 2019).

4.6 | Summary

Naturally elevated seawater CO_2 concentrations altered the composition of prokaryotic and eukaryotic biofilm communities through early successional stages, whilst the richness and evenness of these communities were unaffected. Prokaryotic and eukaryotic communities were more homogeneous under high CO_2 conditions, adding to a growing body of literature reporting increased homogeneity in community composition under high CO_2 conditions. Species turnover, rather than nestedness, was the primary driver differences in prokaryotic and eukaryotic community composition between reference and high CO_2 conditions. The dominance of the toxin-producing golden algae genus *Prymnesium* and the emergence of the large chain-forming diatom *Biddulphia biddulphiana* under high CO_2 conditions add to concerns that ocean acidification may systematically favour harmful algae (Hall-Spencer and Allen 2015; Riebesell *et al.* 2018). This study reveals the ecological patterns that underpin the effect of elevated CO_2 on biofilm communities, which are critical to understanding how these fundamental marine features may respond to near-future conditions.

Acknowledgements

The authors would like to thank the University of Otago Ocean Acidification Research Theme for providing a seed funding grant in support of this project, the technical team at the University of Tsukuba Shimoda Marine Research Center for extensive logistical support, and the captain and crew of the RV Tsukuba II. This project contributes towards the 'International Education and Research Laboratory Program', University of Tsukuba, and we acknowledge funding support from the Ministry of Environment, Government of Japan (Suishinhi: 4RF-1701). The authors declare no conflict of interest.

References

Agostini S, Harvey BP, Wada S *et al.* Ocean acidification drives community shifts towards simplified non-calcified habitats in a subtropical–temperate transition zone. *Sci Rep* 2018;**8**:11354.

Agostini S, Wada S, Kon K *et al.* Geochemistry of two shallow CO_2 seeps in Shikine Island (Japan) and their potential for ocean acidification research. *Reg Stud Mar Sci* 2015;**2**:45–53.

Allen R, Foggo A, Fabricius K *et al.* Tropical CO_2 seeps reveal the impact of ocean acidification on coral reef invertebrate recruitment. *Mar Pollut Bull* 2016;**124**:607–13.

Anderson MJ. A new method for non-parametric multivariate analysis of variance. *Austral Ecol* 2001;**26**:32–46.

Anderson MJ, Ellingsen KE, McArdle BH. Multivariate dispersion as a measure of beta diversity. *Ecol Lett* 2006;**9**:683–93.

Andersson A, Kline D, Edmunds P *et al.* Understanding Ocean Acidification Impacts on Organismal to Ecological Scales. *Oceanography* 2015;**25**:16–27.

Apprill A, Mcnally S, Parsons R *et al.* Minor revision to V4 region SSU rRNA 806R gene primer greatly increases detection of SAR11 bacterioplankton. *Aquat Microb Ecol* 2015;**75**:129–37.

Baselga A. Partitioning the turnover and nestedness components of beta diversity. *Glob Ecol Biogeogr* 2010;**19**:134–43.

Baselga A, Orme CDL. Betapart: An R package for the study of beta diversity. *Methods Ecol Evol* 2012;**3**:808–12.

Brown NE, Therriault TW, Harley CD. Field-based experimental acidification alters fouling community structure and reduces diversity. *J Anim Ecol* 2016;**85**:1328–39.

Brown NEM, Bernhardt JR, Harley CDG. *Energetic Context Determines Species and*

Community Responses to Ocean Acidification., 2020.

Brown NEM, Milazzo M, Rastrick SPS *et al.* Natural acidification changes the timing and rate of succession, alters community structure, and increases homogeneity in marine biofouling communities. *Glob Chang Biol* 2018;**24**:e112–27.

Callahan BJ, McMurdie PJ, Rosen MJ *et al.* DADA2: High-resolution sample inference from Illumina amplicon data. *Nat Methods* 2016a;**13**:581–3.

Callahan BJ, Sankaran K, Fukuyama JA *et al.* Bioconductor Workflow for Microbiome Data Analysis: from raw reads to community analyses. *F1000Research* 2016b;**5**:1492.

Caporaso JG, Lauber CL, Walters WA *et al.* Global patterns of 16S rRNA diversity at a depth of millions of sequences per sample. *Proc Natl Acad Sci* 2011;**108**:4516–22.

Chao A. Nonparametric estimation of the number of classes in a population. *Scand J Stat* 1984:265–70.

Cigliano M, Gambi MC, Rodolfo-Metalpa R *et al.* Effects of ocean acidification on invertebrate settlement at volcanic CO_2 vents. *Mar Biol* 2010;**157**:2489–502.

Connell SD, Doubleday ZA, Foster NR *et al.* The duality of ocean acidification as a resource and a stressor. *Ecology* 2018;**99**:1005–10.

Costerton JW, Lewandowski Z, Caldwell DE *et al.* Microbial biofilms. *Annu Rev Microbiol* 1995;**49**:711–45.

Espinel-Velasco N, Hoffmann L, Agüera A *et al.* Effects of ocean acidification on the settlement and metamorphosis of marine invertebrate and fish larvae: a review. *Mar Ecol Prog Ser* 2018;**606**:237–57.

Espinel-Velasco N, Tobias-Hünefeldt SP, Karelitz S *et al.* Reduced seawater pH alters marine biofilms with impacts for marine polychaete larval settlement. *Mar Environ Res* 2021;**167**, DOI: 10.1016/j.marenvres.2021.105291.

Fabricius KE, Kluibenschedl A, Harrington L *et al.* In situ changes of tropical crustose

coralline algae along carbon dioxide gradients. *Sci Rep* 2015;**5**:9537.

Fabricius KE, Langdon C, Uthicke S *et al.* Losers and winners in coral reefs acclimatized to elevated carbon dioxide concentrations. *Nat Clim Chang* 2011;**1**:165–9.

Fabricius KE, Noonan SHC, Abrego D *et al.* Low recruitment due to altered settlement substrata as primary constraint for coral communities under ocean acidification. *Proc R Soc B Biol Sci* 2017;**284**:20171536.

Fistarol GO, Legrand C, Granéli E. Allelopathic effect of Prymnesium parvum on a natural plankton community. *Mar Ecol Prog Ser* 2003;**255**:115–25.

Flemming H-C, Wingender J, Szewzyk U *et al.* Biofilms: an emergent form of bacterial life. *Nat Rev Microbiol* 2016;**14**:563–75.

Flemming H-C, Wuertz S. Bacteria and archaea on Earth and their abundance in biofilms. *Nat Rev Microbiol* 2019, DOI: 10.1038/s41579-019-0158-9.

Flemming HC, Wingender J. The biofilm matrix. *Nat Rev Microbiol* 2010;**8**:623–33.

Galland G, Pennebaker S. A benthic diatom bloom in the Gulf of California, Mexico. *BioInvasions Rec* 2012;**1**:65–9.

Griffith JC, Lee WG, Orlovich DA *et al.* Contrasting bacterial communities in two indigenous Chionochloa (Poaceae) grassland soils in New Zealand. Wilson BA (ed.). *PLoS One* 2017;**12**:e0179652.

Guillou L, Bachar D, Audic S *et al.* The Protist Ribosomal Reference database (PR2): A catalog of unicellular eukaryote Small Sub-Unit rRNA sequences with curated taxonomy. *Nucleic Acids Res* 2013;**41**:597–604.

Hall-Spencer J, Allen R. The impact of CO_2 emissions on “nuisance” marine species. *Res Reports Biodivers Stud* 2015:33.

Hall-Spencer JM, Harvey BP. Ocean acidification impacts on coastal ecosystem services due to habitat degradation. *Emerg Top Life Sci* 2019;**3**:197–206.

Hall-Spencer JM, Rodolfo-Metalpa R, Martin S *et al.* Volcanic carbon dioxide vents show ecosystem effects of ocean acidification. *Nature* 2008;**454**:96–9.

Harvey BP, Agostini S, Kon K *et al.* Diatoms dominate and alter marine food-webs when CO_2 rises. *Diversity* 2019;**11(12)**:242.

Harvey BP, Agostini S, Wada S *et al.* Dissolution: the Achilles' heel of the triton shell in an acidifying ocean. *Front Mar Sci* 2018;**5**:371.

Harvey BP, Allen R, Agostini S *et al.* Feedback mechanisms stabilise degraded turf algal systems at a CO_2 seep site. *Commun Biol* 2021a;**4**:219.

Harvey BP, Kon K, Agostini S *et al.* Ocean acidification locks algal communities in a species-poor early successional stage. *Glob Chang Biol* 2021b:gcb.15455.

Hassenrück C, Tegetmeyer HE, Ramette A *et al.* Minor impacts of reduced pH on bacterial biofilms on settlement tiles along natural pH gradients at two CO_2 seeps in Papua New Guinea. *ICES J Mar Sci J du Cons* 2017;**74**:978–87.

Hoegh-Guldberg O, Poloczanska E, Brewer P *et al.* The Ocean. *Climate Change 2014: Impacts, Adaptation, and Vulnerability. Part A: Global and Sectoral Aspects. Contribution of Working Group II to the Fifth Assessment Report of the Intergovernmental Panel on Climate Change*. Cambridge, United Kingdom, and New York, NY, USA, 2014, 1655–731.

Jeffrey SW t, Humphrey GF. New spectrophotometric equations for determining chlorophylls a, b, c1 and c2 in higher plants, algae and natural phytoplankton. *Biochem und Physiol der Pflanz* 1975;**167**:191–4.

Johnson V, Brownlee C, Milazzo M *et al.* Marine Microphytobenthic Assemblage Shift along a Natural Shallow-Water CO_2 Gradient Subjected to Multiple Environmental Stressors. *J Mar Sci Eng* 2015;**3**:1425–47.

Johnson VR, Brownlee C, Rickaby REM *et al.* Responses of marine benthic microalgae to

elevated CO_2. *Mar Biol* 2013;**160**:1813–24.

Kerfahi D, Hall-Spencer JM, Tripathi BM *et al.* Shallow Water Marine Sediment Bacterial Community Shifts Along a Natural CO_2 Gradient in the Mediterranean Sea Off Vulcano, Italy. *Microb Ecol* 2014;**67**:819–28.

Kerfahi D, Harvey BP, Agostini S *et al.* Responses of Intertidal Bacterial Biofilm Communities to Increasing pCO_2. *Mar Biotechnol* 2020, DOI: 10.1007/s10126-020-09958-3.

De Kievit TR. Quorum sensing in Pseudomonas aeruginosa biofilms. *Environ Microbiol* 2009;**11**:279–88.

Kroeker KJ, Micheli F, Gambi MC. Ocean acidification causes ecosystem shifts via altered competitive interactions. *Nat Clim Chang* 2012;**3**:156–9.

Lidbury I, Johnson V, Hall-Spencer JM *et al.* Community-level response of coastal microbial biofilms to ocean acidification in a natural carbon dioxide vent ecosystem. *Mar Pollut Bull* 2012;**64**:1063–6.

Mackey K, Morris JJ, Morel F *et al.* Response of Photosynthesis to Ocean Acidification. *Oceanography* 2015;**25**:74–91.

Manning SR, La Claire JW. Prymnesins: Toxic metabolites of the golden alga, Prymnesium parvum Carter (Haptophyta). *Mar Drugs* 2010;**8**:678–704.

Massana R, Gobet A, Audic S *et al.* Marine protist diversity in European coastal waters and sediments as revealed by high-throughput sequencing. *Environ Microbiol* 2015;**17**:4035–49.

McMurdie PJ, Holmes S. Phyloseq: An R Package for Reproducible Interactive Analysis and Graphics of Microbiome Census Data. *PLoS One* 2013;**8**:e61217.

Nelson KS, Baltar F, Lamare MD *et al.* Ocean acidification affects microbial community and invertebrate settlement on biofilms. *Sci Rep* 2020;**10**:1–9.

Oksanen J, Blanchet FG, Friendly M *et al.* vegan: Community Ecology Package. 2016.

Olden JD, Poff NLR, Douglas MR *et al.* Ecological and evolutionary consequences of biotic homogenization. *Trends Ecol Evol* 2004;**19**:18–24.

Parada AE, Needham DM, Fuhrman JA. Every base matters: assessing small subunit rRNA primers for marine microbiomes with mock communities, time series and global field samples. *Environ Microbiol* 2016;**18**:1403–14.

Pielou EC. The measurement of diversity in different types of biological collections. *J Theor Biol* 1966;**13**:131–44.

Pohlon E, Marxsen J, Küsel K. Pioneering bacterial and algal communities and potential extracellular enzyme activities of stream biofilms. *FEMS Microbiol Ecol* 2010;**71**:364–73.

Porzio L, Buia MC, Hall-Spencer JM. Effects of ocean acidification on macroalgal communities. *J Exp Mar Bio Ecol* 2011;**400**:278–87.

Porzio L, Garrard SL, Buia MC. The effect of ocean acidification on early algal colonization stages at natural CO_2 vents. *Mar Biol* 2013;**160**:2247–59.

Prosser KN, Valenti TW, Hayden NJ *et al.* Low pH preempts bloom development of a toxic haptophyte. *Harmful Algae* 2012;**20**:156–64.

Quast C, Pruesse E, Yilmaz P *et al.* The SILVA ribosomal RNA gene database project: Improved data processing and web-based tools. *Nucleic Acids Res* 2013;**41**:590–6.

Rajaram S, Oono Y. NeatMap - non-clustering heat map alternatives in R. *BMC Bioinformatics* 2010;**11**:45.

Riebesell U, Aberle-Malzahn N, Achterberg EP *et al.* Toxic algal bloom induced by ocean acidification disrupts the pelagic food web. *Nat Clim Chang* 2018;**8**:1082–6.

Roelke DL, Barkoh A, Brooks BW *et al.* A chronicle of a killer alga in the west: ecology, assessment, and management of Prymnesium parvum blooms. *Hydrobiologia*

2016;**764**:29–50.

Russell BD, Connell SD, Findlay HS *et al.* Ocean acidification and rising temperatures may increase biofilm primary productivity but decrease grazer consumption. *Philos Trans R Soc Lond B Biol Sci* 2013;**368**:20120438.

Sanli K, Bengtsson-Palme J, Nilsson RH *et al.* Metagenomic sequencing of marine periphyton: taxonomic and functional insights into biofilm communities. *Front Microbiol* 2015;**6**:1–14.

Seoane S, Riobó P, Franco J. Haemolytic activity in different species of the genus Prymnesium (Haptophyta). *J Mar Biol Assoc United Kingdom* 2017;**97**:491–6.

Stoeck T, Bass D, Nebel M *et al.* Multiple marker parallel tag environmental DNA sequencing reveals a highly complex eukaryotic community in marine anoxic water. *Mol Ecol* 2010;**19**:21–31.

Taylor JD, Ellis R, Milazzo M *et al.* Intertidal epilithic bacteria diversity changes along a naturally occurring carbon dioxide and pH gradient. *FEMS Microbiol Ecol* 2014;**89**:670–8.

Team RC. R: A language and environment for statistical computing. 2013.

Thompson RC, Norton TA, Hawkins SJ. Physical stress and biological control regulate the producer–consumer balance in intertidal biofilms. *Ecology* 2004;**85**:1372–82.

Tran C, Hadfield MG. Larvae of Pocillopora damicornis (Anthozoa) settle and metamorphose in response to surface-biofilm bacteria. *Mar Ecol Prog Ser* 2011;**433**:85–96.

Wang Q, Garrity GM, Tiedje JM *et al.* Naïve Bayesian classifier for rapid assignment of rRNA sequences into the new bacterial taxonomy. *Appl Environ Microbiol* 2007;**73**:5261–7.

Witt V, Wild C, Anthony KRN *et al.* Effects of ocean acidification on microbial community composition of, and oxygen fluxes through, biofilms from the Great Barrier Reef.

Environ Microbiol 2011a;**13**:2976–89.

Witt V, Wild C, Anthony KRN *et al.* Effects of ocean acidification on microbial community composition of, and oxygen fluxes through, biofilms from the Great Barrier Reef. *Environ Microbiol* 2011b;**13**:2976–2989.

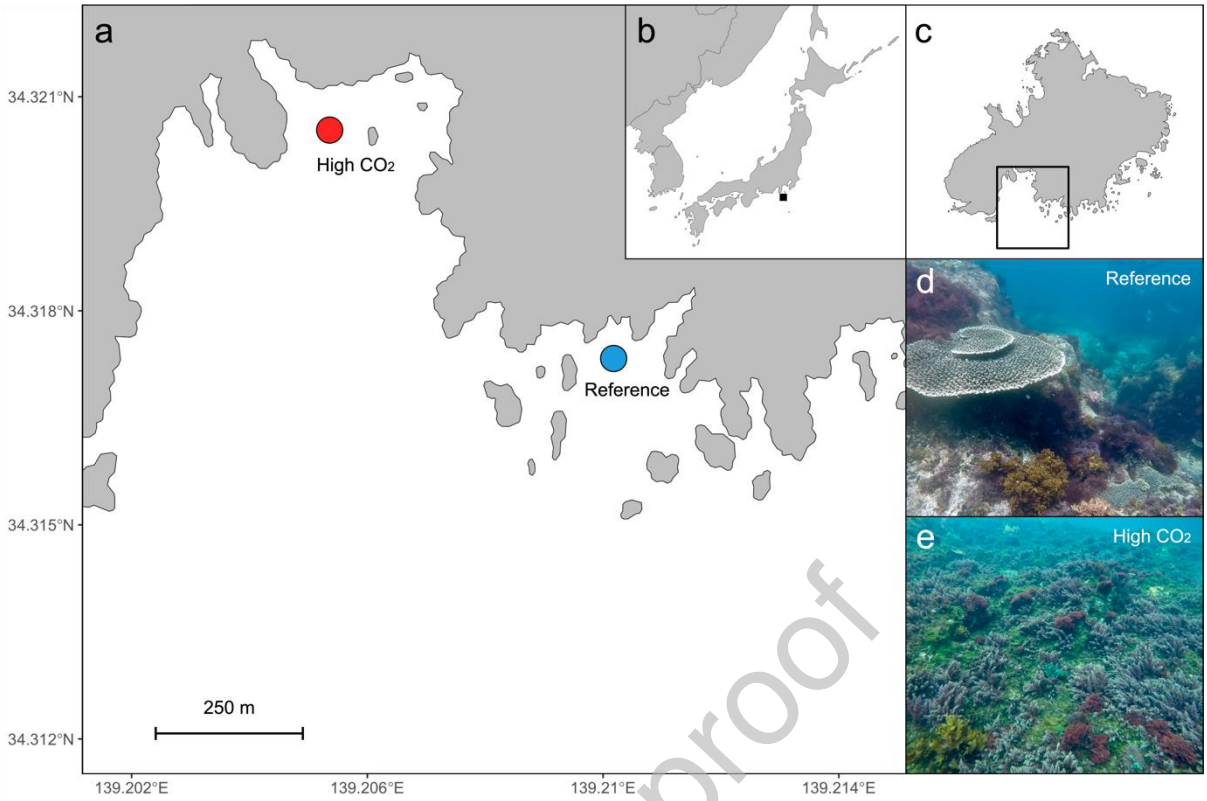

Figure 1. (a) Map of Mikawa Bay, at Shikine Island. Reference and high CO_2 sites are indicated by blue and red points, respectively. (b) Map of Japan with a black bounding-box around Shikine Island. (c) Map of Shikine Island, with a black bounding-box around the Mikawa Bay region. (d, e) Photographic insets showing representative seascapes at the reference and high CO_2 sites, taken during sampling for this study.

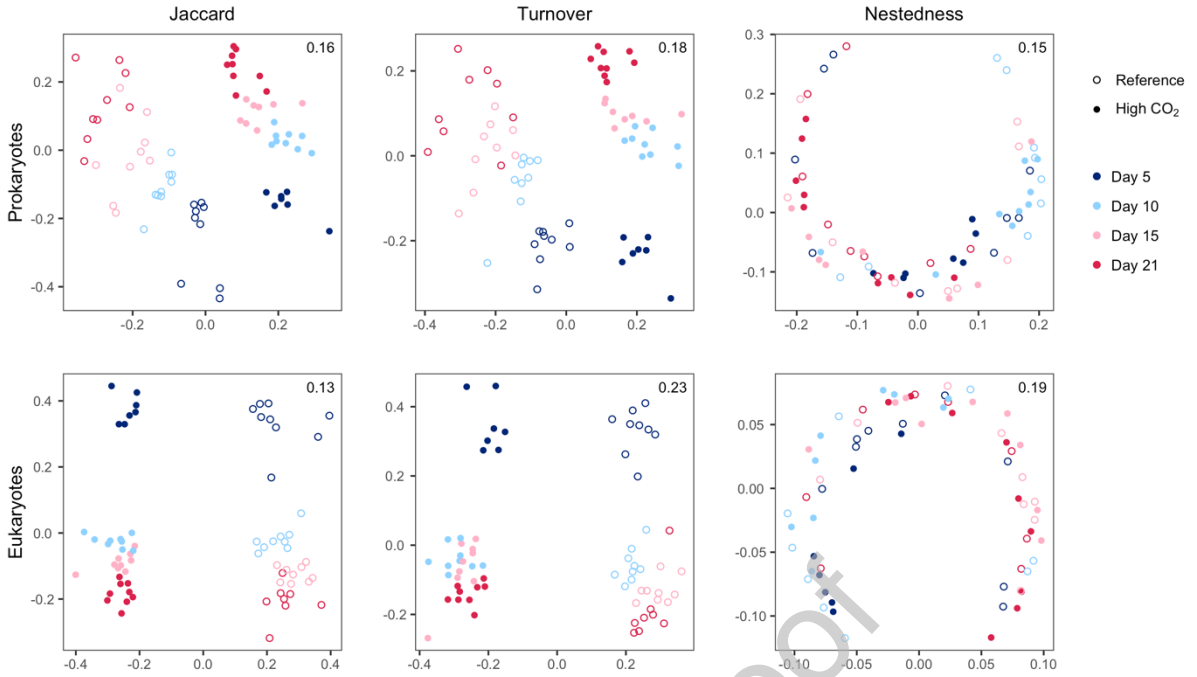

Figure 2. nMDS ordinations of prokaryotic (16S rRNA gene) and eukaryotic (18S rRNA gene) biofilm community composition under reference (open circles) and high CO_2 (filled circles) conditions at each time point, based on Jaccard dissimilarity, the turnover component of Jaccard dissimilarity, and the nestedness component of Jaccard dissimilarity, respectively. Stress values are indicated in the upper right corner of each plot.

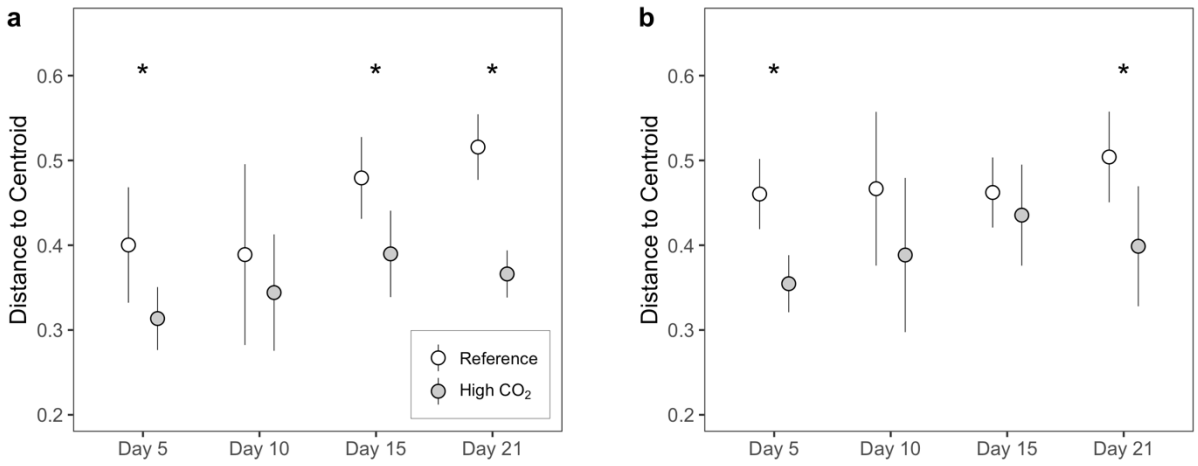

Figure 3. Distance to centroid (compositional variability) based on Jaccard dissimilarity in (a) prokaryotic and (b) eukaryotic biofilm communities under reference (n = 9) and high CO_2 (n = 9) conditions at each time point. Points represent the mean value, error bars represent the standard deviation. Asterisks denote time points where distance to centroid differs significantly between sites ($p < 0.05$).

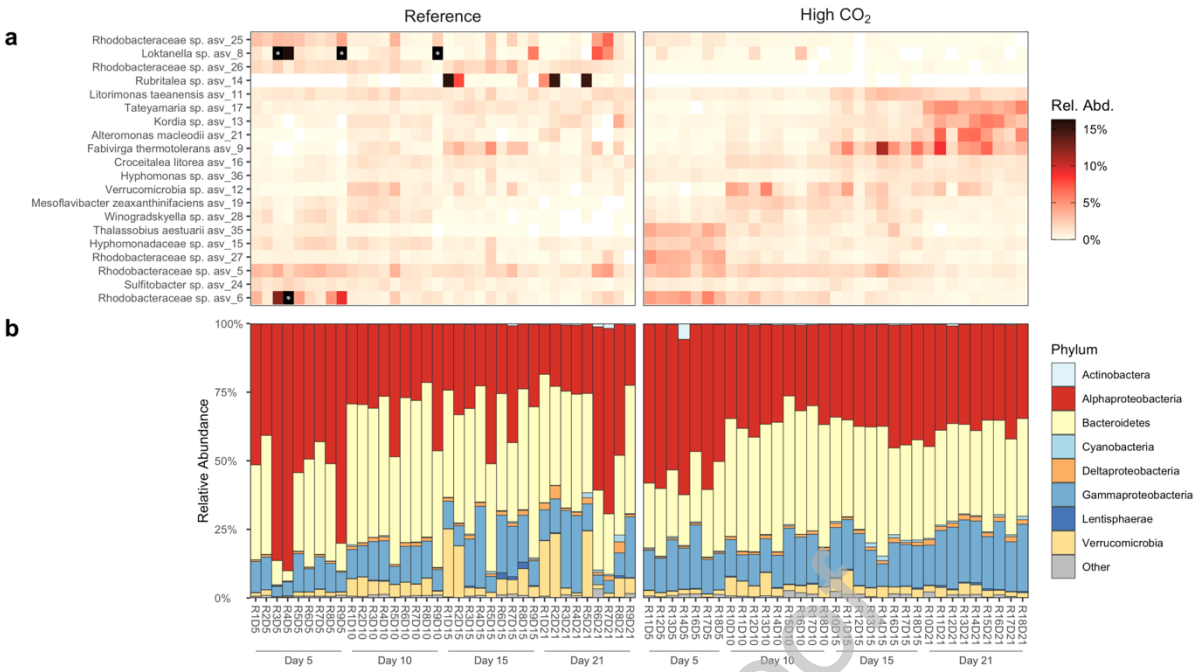

Figure 4. (a) Heatmap of the 20 most abundant ASVs in prokaryotic biofilms under reference and high CO_2 conditions. Taxonomic classification of ASVs represents the best match within the NCBI database (Table S1). ASVs are ordered according to the neatmap algorithm (Rajaram and Oono 2010). Colour bar indicates the proportion of reads in each sample attributed to a particular ASV (relative abundance). White asterisk indicates relative abundance which exceeds the range of the colour scale. (b) Phylum level composition of prokaryotic biofilm communities under reference and high CO_2 conditions.

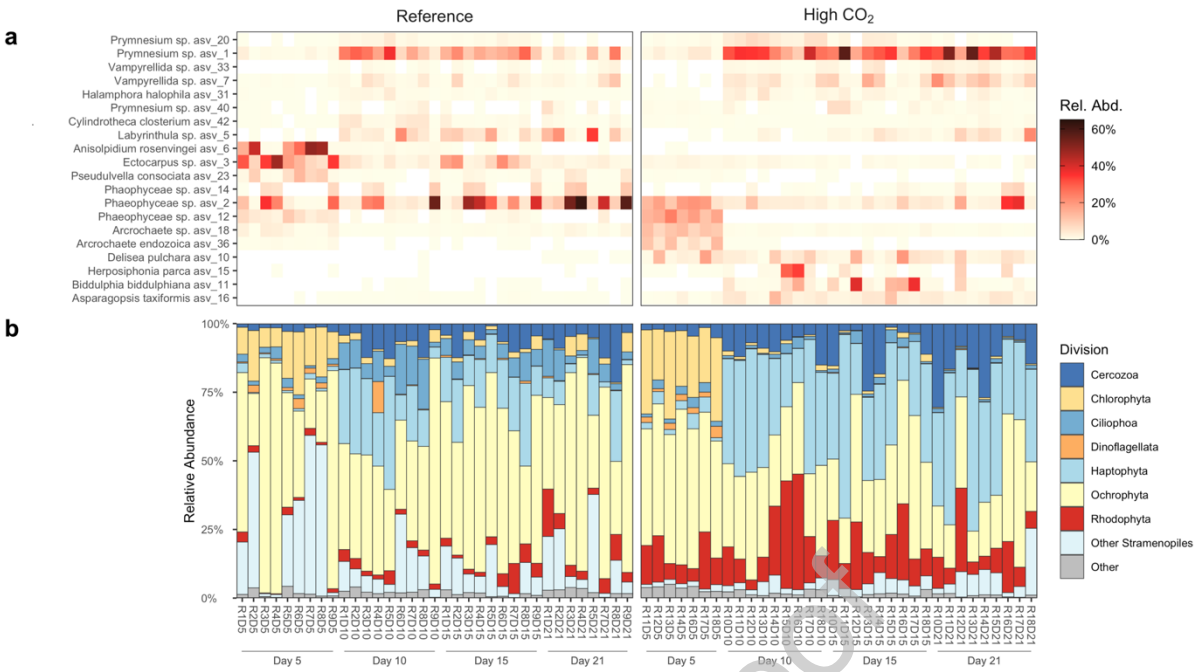

Figure 5. (a) Heatmap of the 20 most abundant eukaryotic ASVs in biofilms under reference and high CO_2 conditions. Taxonomic classification of ASVs represents the best match within the NCBI database (Table S1). ASVs are ordered according to the neatmap algorithm (Rajaram and Oono 2010). Colour bar indicates the proportion of reads in each sample attributed to a particular ASV (relative abundance). (b) Division level composition of eukaryotic biofilm communities under reference and high CO_2 conditions.

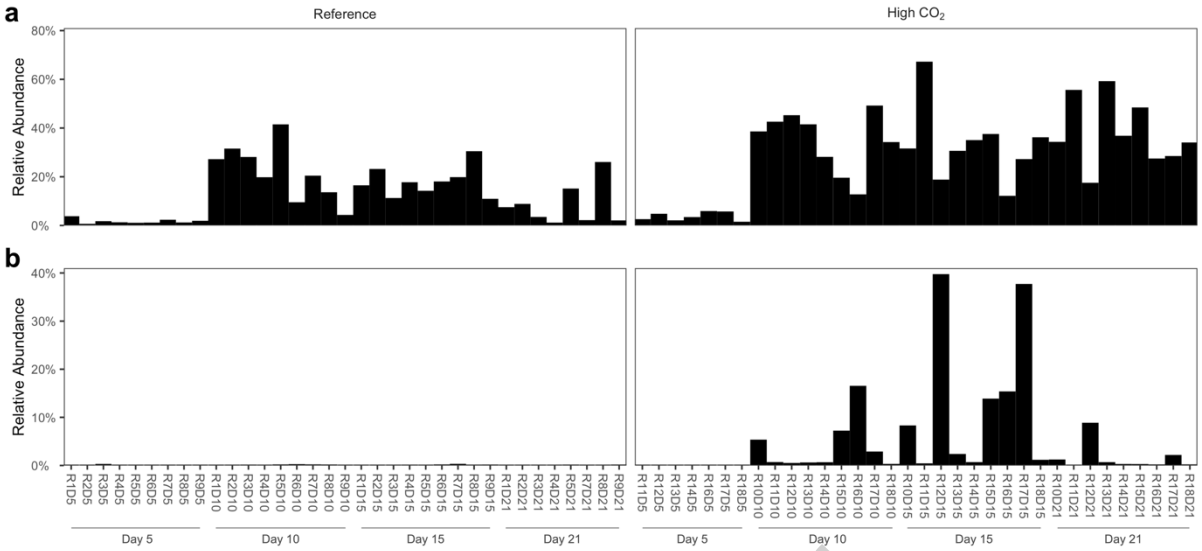

Figure 6. Bar plot of the relative abundance of summed (a) *Prymnesium sp.* reads and (b) *Biddulphia biddulphiana* reads under reference and high CO_2 conditions at each time point, based on 18S rRNA gene sequences.

Tables

Table 1. Carbonate chemistry under reference and high CO_2 conditions at Shikine Island, Japan. The pHT (Reference, n = 1964; High CO_2, n = 10818), salinity (Reference, n = 1964; High CO_2, n = 10818), and total alkalinity (Reference, n = 56; High CO_2, n = 47) are measured parameters. All measurements were taken at 5-6 m depth. All other values were calculated from measured values using CO2SYS (Pierrot et al. 2006). Values shown are mean ± standard deviation. Table reproduced from Harvey et al. (2021b).

	Reference	High CO_2
pH total	8.137 ± 0.056	7.788 ± 0.106
Salinity (psu)	34.504 ± 0.427	34.351 ± 0.484
A_T (μmol kg^{-1})	2264.29 ± 15.34	2268.33 ± 19.45
pCO_2 (μatm)	316.057 ± 47.466	841.148 ± 291.762
DIC (μmol kg^{-1})	1962.694 ± 34.376	2125.785 ± 39.381
HCO_3^- (μmol kg^{-1})	1740.629 ± 55.084	1984.889 ± 52.510
CO_3^{2-} (μmol kg^{-1})	211.979 ± 22.221	115.150 ± 21.308
Ω calcite	5.087 ± 0.534	2.771 ± 0.512
Ω aragonite	3.301 ± 0.348	1.805 ± 0.336

Table 2. Global and pairwise PERMANOVA comparisons of prokaryotic and eukaryotic biofilm community composition between sites and time points based on Jaccard dissimilarity, the turnover component of Jaccard dissimilarity, and nestedness component of Jaccard dissimilarity, respectively.

	Jaccard Dissimilarity			Turnover			Nestedness		
	Pseudo-*F*	R^2	*p*	Pseudo-*F*	R^2	*p*	Pseudo-*F*	R^2	*p*
Prokaryotes									
Condition	16.48	0.16	**0.001**	30.242	0.24	**0.001**	-16.607	-0.035	1
Time	6.07	0.17	**0.001**	7.598	0.181	**0.001**	1.042	0.066	0.434
Condition x Time	2.87	0.08	**0.001**	3.959	0.094	**0.001**	0.003	0	0.87
Reference-High CO_2 (Day 5)	4.156	0.229	**0.001**	6.453	0.316	**0.002**	-1.877	-0.155	1
Reference-High CO_2 (Day 10)	9.037	0.361	**0.001**	14.768	0.48	**0.001**	-5.396	-0.509	1
Reference-High CO_2 (Day 15)	5.953	0.284	**0.001**	10.949	0.42	**0.001**	-4.966	-0.495	1
Reference-High CO_2 (Day 21)	6.402	0.286	**0.001**	10.461	0.395	**0.001**	-5.338	-0.501	1
Day 5-Day 10 (Reference)	3.532	0.181	**0.002**	4.684	0.226	**0.001**	1.533	0.087	0.261
Day 10-Day 15 (Reference)	2.506	0.135	**0.003**	2.656	0.142	**0.003**	3.866	0.195	0.059
Day 15-Day 21 (Reference)	1.781	0.1	**0.026**	2.01	0.116	**0.015**	1.482	0.085	0.243
Day 5-Day 10 (High CO_2)	5.813	0.293	**0.001**	6.84	0.328	**0.001**	-2.702	-0.239	0.998
Day 10-Day 15 (High CO_2)	3.26	0.179	**0.002**	2.244	0.13	**0.017**	3.729	0.199	0.082
Day 15-Day 21 (High CO_2)	3.096	0.171	**0.001**	4.247	0.221	**0.001**	-0.38	-0.026	0.937
Eukaryotes									
Condition	12.66	0.14	**0.001**	17.5	0.178	**0.001**	-22.75	-0.553	1
Time	3.81	0.12	**0.001**	4.36	0.133	**0.001**	-0.38	-0.028	0.889
Condition x Time	2.24	0.07	**0.001**	2.25	0.068	**0.001**	1.351	0.098	0.356
Reference-High CO_2 (Day 5)	3.032	0.178	**0.001**	2.998	0.176	**0.001**	3.783	0.213	0.06
Reference-High CO_2 (Day 10)	5.928	0.27	**0.001**	8.224	0.34	**0.001**	-6.481	-0.681	1
Reference-High CO_2 (Day 15)	5.626	0.26	**0.001**	7.054	0.306	**0.001**	-6.789	-0.737	1
Reference-High CO_2 (Day 21)	5.016	0.251	**0.001**	6.641	0.307	**0.001**	-5.186	-0.528	1
Day 5-Day 10 (Reference)	3.393	0.175	**0.001**	4.413	0.216	**0.001**	-3.624	-0.293	1
Day 10-Day 15 (Reference)	2.053	0.114	**0.002**	1.752	0.099	**0.002**	3.522	0.18	0.077
Day 15-Day 21 (Reference)	1.422	0.066	**0.036**	1.584	0.096	**0.034**	0.44	0.029	0.611
Day 5-Day 10 (High CO_2)	3.89	0.217	**0.001**	4.273	0.234	**0.001**	-1.333	-0.105	0.991
Day 10-Day 15 (High CO_2)	1.909	0.107	**0.001**	1.639	0.093	**0.005**	7.44	0.317	**0.02**
Day 15-Day 21 (High CO_2)	1.657	0.094	**0.001**	1.727	0.097	**0.002**	1.852	0.104	0.212

Supplementary Material

Table S1. Global and pairwise PERMANOVA comparisons of prokaryotic and eukaryotic biofilm community composition between sites and time points based on Bray-Curtis dissimilarity.

	Bray-Curtis Dissimilarity		
	Pseudo-*F*	R^2	*p*
Prokaryotes			
Condition	24.01	0.18	**0.001**
Time	11.23	0.26	**0.001**
Condition x Time	4.31	0.10	**0.001**
Reference-High CO_2 (Day 5)	9.718	0.410	**0.001**
Reference-High CO_2 (Day 10)	12.549	0.440	**0.001**
Reference-High CO_2 (Day 15)	7.695	0.339	**0.001**
Reference-High CO_2 (Day 21)	8.453	0.346	**0.001**
Day 5-Day 10 (Reference)	7.211	0.311	**0.001**
Day 10-Day 15 (Reference)	2.578	0.139	**0.007**
Day 15-Day 21 (Reference)	1.532	0.087	0.123
Day 5-Day 10 (High CO_2)	15.009	0.517	**0.001**
Day 10-Day 15 (High CO_2)	5.696	0.275	**0.001**
Day 15-Day 21 (High CO_2)	6.788	0.312	**0.001**
Eukaryotes			
Condition	24.15	0.18	**0.001**
Time	11.20	0.15	**0.001**
Condition x Time	4.70	0.10	**0.001**
Reference-High CO_2 (Day 5)	11.649	0.454	**0.001**
Reference-High CO_2 (Day 10)	8.7893	0.355	**0.001**
Reference-High CO_2 (Day 15)	9.367	0.369	**0.001**
Reference-High CO_2 (Day 21)	8.007	0.348	**0.002**
Day 5-Day 10 (Reference)	10.752	0.402	**0.001**
Day 10-Day 15 (Reference)	2.176	0.120	**0.045**
Day 15-Day 21 (Reference)	2.053	0.120	0.084
Day 5-Day 10 (High CO_2)	12.602	0.474	**0.001**
Day 10-Day 15 (High CO_2)	2.252	0.123	**0.041**
Day 15-Day 21 (High CO_2)	2.527	0.136	**0.023**

Table S2. Taxonomic classification of top 20 prokaryotic and eukaryotic ASVs according to the NCBI database (BLASTn; accessed May 2020). Top hit based on E-value is displayed. Where multiple sequences returned maximal E-values, up to three sequences are listed.

ASV ID	NCBI Match ID	Max Score	Total Score	Query Cover	E value	Per. Ident	Accession
Prokaryotes							
Rhodobacteraceae sp. asv_25	Thalassobacter sp. AI_3	459	459	1	4E-125	0.9921	LC543481.1
	Octadecabacter sp. strain CP135	459	459	1	4E-125	0.9921	MH061224.1
	Pseudooctadecabacter sp. strain JL3664	459	459	1	4E-125	0.9921	KX989201.1
Loktanella sp. asv_8	Loktanella sp. SW2211	470	470	1	2E-128	1	LR722710.1
	Loktanella tamlensis isolate ZB_2_224	470	470	1	2E-128	1	LR722708.1
	Loktanella sediminilitoris isolate HaHa_3_185	470	470	1	2E-128	1	LR722707.1
Rhodobacteraceae sp. asv_26	Tateyamaria omphalii strain CM_D10_26	470	470	1	2E-128	1	MT452294.1
	Pseudooceanicola nitratireducens strain CM_D10_24	470	470	1	2E-128	1	MT452292.1
	Tateyamaria omphalii strain CM_D1_26	470	470	1	2E-128	1	MT449067.1
Rubritalea sp. asv_14	Rubritalea sp. shu-10-MA45-1	425	425	1	4E-115	0.9685	AB543682.1
Litorimonas taeanensis asv_11	Litorimonas sp. strain WHOIMSCC53216RPlateR77272E08	470	470	1	2E-128	1	MF599746.1
	Litorimonas taeanensis strain G5	470	470	1	2E-128	1	NR_116589.1
Tateyamaria sp. asv_17	Tateyamaria sp. KMU-156	464	464	1	8E-127	0.9961	LC464518.1
	Tateyamaria omphalii strain 3 HE 3A	464	464	1	8E-127	0.9961	MK224714.1
	Tateyamaria sp. strain Alg231-49	464	464	1	8E-127	0.9961	KY363630.1
Kordia sp. asv_13	Kordia ulvae strain SC2	470	470	1	2E-128	1	NR_149793.1
	Kordia algicida	470	470	1	2E-128	1	FJ015036.1
Alteromonas macleoidii asv_21	Alteromonas macleodii	425	425	1	4E-115	0.9685	FN811296.1
	Alteromonas macleodii	425	425	1	4E-115	0.9685	AF173965.1
Fabivirga thermotolerans asv_9	Fabivirga thermotolerans strain A-4	364	364	1	9E-97	0.9252	NR_148597.1
Corceitalea litorea asv_16	Croceitalea litorea strain CBA3205	470	470	1	2E-128	1	NR_145873.1
Hyphomonas sp. asv_36	Hyphomonas sp. Mor2	448	448	1	9E-122	0.9843	CP017718.1
Verrucomicrobia sp. asv_12	Verrucomicrobia bacterium P1_50_6AA2	425	425	1	4E-115	0.9685	KT906996.1
	Verrucomicrobia bacterium P1_50_6AA1	425	425	1	4.00E-115	0.9685	KT906995.1
	Verrucomicrobia bacterium IMCC11022	425	425	1	4E-115	0.9685	KJ411775.1
Mesoflavibacter zeaxanthinifaciens asv_19	Mesoflavibacter zeaxanthinifaciens isolate 32-C4	436	436	1	2E-118	0.9764	LK022170.1
	Mesoflavibacter zeaxanthinifaciens isolate 31-C4	436	436	1	2E-118	0.9764	LK022169.1
Winogradskyella sp. asv_28	Winogradskyella sp. PC-19	470	940	1	2E-128	1	CP019332.1
Thalassobius aestuarii asv_35	Thalassobius aestuarii strain F84013	459	459	1	4E-125	0.9921	HQ908719.1
Hyphomonadaceae sp. asv_15	Hyphomonadaceae bacterium strain H05Y-209	459	459	1	4E-125	0.9921	MK493580.1
	Hyphomonas sp. DG1513	459	459	1	4E-125	0.9921	KC295391.1
	Hyphomonas sp. DG1448	459	459	1	4E-125	0.9921	KC295358.1

Rhodobacteraceae sp. asv_27	Pseudopelagicola sp. strain LW3-34	453	453	1	2E-123	0.9882	MG818318.1
	Aliiroseovarius sp. strain PrR0016	453	453	1	2E-123	0.9882	MF948946.1
	Oceanicola sp. LZD010	453	453	1	2E-123	0.9882	KP639146.1
Rhodobacteraceae sp. asv_5	Jannaschia sp. UDC482	470	470	1	2E-128	1	HM032013.1
	Thalassobius sp. UST061013-004	470	470	1	2E-128	1	EF587951.1
Sulfitobacter sp. asv_24	Sulfitobacter porphyrae strain ZFX1	470	470	1	2E-128	1	MT012050.1
	Sulfitobacter pacificus isolate R2A112_6_28	470	470	1	2E-128	1	LR722702.1
	Sulfitobacter porphyrae strain S12B-106	470	470	1	2E-128	1	MK493601.1
Rhodobacteraceae sp. asv_6	Maritimibacter sp. DP07	470	470	1	2E-128	1	MN381951.1
	Planktotalea frisia isolate HaHa_3_181	470	470	1	2E-128	1	LR722720.1
	Rhodobacteraceae bacterium DN153	470	470	1	2E-128	1	LC193134.1
Eukaryotes							
Prymnesium sp. asv_20	Prymnesium pienaarii strain Xmm1S4	680	680	1	0	0.9885	KY054990.1
	Prymnesium simplex isolate DHmm2W3	680	680	1	0	0.9895	KU561118.1
	Prymnesium pienaarii isolate DHmm2W1	680	680	1	0	0.9895	KU561110.1
Prymnesium sp. asv_1	Prymnesium pienaarii strain Xmm1S4	675	675	1	0	0.9869	KY054990.1
	Prymnesium simplex isolate DHmm2W3	675	675	1	0	0.9869	KU561118.1
	Prymnesium pienaarii isolate DHmm2W1	675	675	1	0	0.9869	KU561110.1
Vampyrellida sp. asv_33	Vampyrellida sp. CAraX	243	243	1	7E-60	0.7864	KC779514.1
Vampyrellida sp. asv_7	Vampyrellida sp. CAraX	237	237	1	3E-58	0.7839	KC779514.1
Halamphora halophila asv_31	Halamphora halophila isolate 9995-AMPH185	656	656	1	0	0.9839	MG027335.1
Prymnesium sp. asv_40	Prymnesium faveolatum strain ALGO HAP79	704	704	1	0	1	AM491005.2
	Prymnesium calathiferum strain CCMP 707	704	704	1	0	1	AM491008.2
	Prymnesium annuliferum strain ALGO HAP47	704	704	1	0	1	AM491007.2
Cylindrotheca closterium asv_42	Cylindrotheca closterium strain UPMC-A0076	704	704	1	0	1	MH166733.1
	Cylindrotheca closterium	704	704	1	0	1	KY045848.1
	Cylindrotheca sp. isolate UTKSA0079	704	704	1	0	1	KX981848.1
Labyrinthula sp. asv_5	Labyrinthula sp. OVP-2019a strain	448	448	1	1E-121	0.8877	MN101174.1
Anisolpidium rosenvingei asv_6	Anisolpidium rosenvingei isolate Roscoff 2014	676	676	1	0	0.9844	KU764783.1
	Anisolpidium rosenvingei isolate A_ros_Perharidy_2015-4	676	676	1	0	0.9844	KU752534.1
Ectocarpus sp. asv_3	Ectocarpus fasciculatus	728	728	1	0	1	KU752533.1
	Ectocarpus fasciculatus strain Ec395	728	728	1	0	1	FN564441.1
	Ectocarpus siliculosus strain 3477	728	728	1	0	1	AY307398.1
Pseudulvella consociata asv_23	Pseudulvella consociata culture-collection CCMP:1676	640	640	1	2E-179	0.971	JF680953.1
Phaeophyceae sp. asv_14	Adenocystis utricularis	662	662	1	0	0.9695	KY987592.1
	Halothrix ambigua	662	662	1	0	0.9695	AY232607.1
	Myrionema strangulans	662	662	1	0	0.9695	AY232605.1

Phaeophyceae sp. asv_2	Adenocystis utricularis	706	706	1	0	0.9898	KY987592.1
	Halothrix ambigua	706	706	1	0	0.9898	AY232607.1
	Myrionema strangulans	706	706	1	0	0.9898	AY232605.1
Phaeophyceae sp. asv_12	Adenocystis utricularis	721	721	1	0	0.9975	KY987592.1
	Halothrix ambigua	721	721	1	0	0.9975	AY232607.1
	Myrionema strangulans	721	721	1	0	0.9975	AY232605.1
Arcrochaete sp. asv_18	Acrochaete sp. RCC2960	701	701	1	0	1	KT860928.1
	Ulvella leptochaete strain CCAP 6037/1, isolate 11-1-2/080211-1	701	701	1	0	1	LM653280.1
	Acrochaete leptochaete voucher AST2008103001-1	701	701	1	0	1	JN104106.1
Arcrochaete endozoica asv_36	Acrochaete endozoica	684	684	1	0	0.9921	AY205327.1
Delisea pulchara asv_10	Delisea pulchra voucher G0370	675	675	1	0	0.9869	AY437645.1
Heroposiphonia parca asv_15	Herposiphonia parca voucher CH426	710	710	1	0	1	JX828166.1
Biddulphia biddulphiana asv_11	Biddulphia biddulphiana strain TongYeongLNG Bbidd	710	710	1	0	1	MN917241.1
Asparagopsis taxiformis asv_16	Asparagopsis taxiformis voucher Florida	712	712	1	0	1	MN547336.1
	Asparagopsis taxiformis voucher Fiji	712	712	1	0	1	MN547335.1
	Asparagopsis taxiformis voucher Hawaii	712	712	1	0	1	MN547334.1

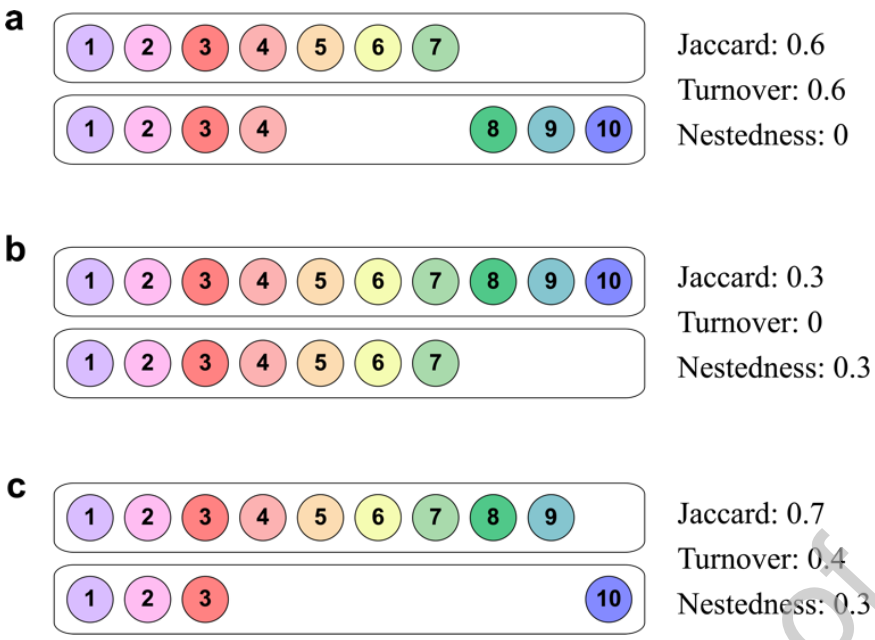

Figure S1. Adapted from Baselga et al. (2009). Conceptual example of the additive decomposition of Jaccard dissimilarity between pairs of communities when beta-diversity is underpinned exclusively by turnover (a), exclusively by nestedness (b), or by a combination of nestedness and turnover (c). Each coloured circle represents a distinct microbial ASV. The Jaccard dissimilarity and its turnover and nestedness components are calculated as follows (Baselga and Orme 2012):

$$Jaccard = \frac{b+c}{a+b+c} \equiv \frac{2b}{2b+a} + \left(\frac{c-b}{a+b+c}\right)\left(\frac{a}{2b+a}\right)$$

$$Turnover = \frac{2b}{2b+a}$$

$$Nestedness = \left(\frac{c-b}{a+b+c}\right)\left(\frac{a}{2b+a}\right)$$

Where a is the number of species shared between the pair of communities, b is the number of species unique to the least speciose community, and c is the number of species unique to the most speciose community.

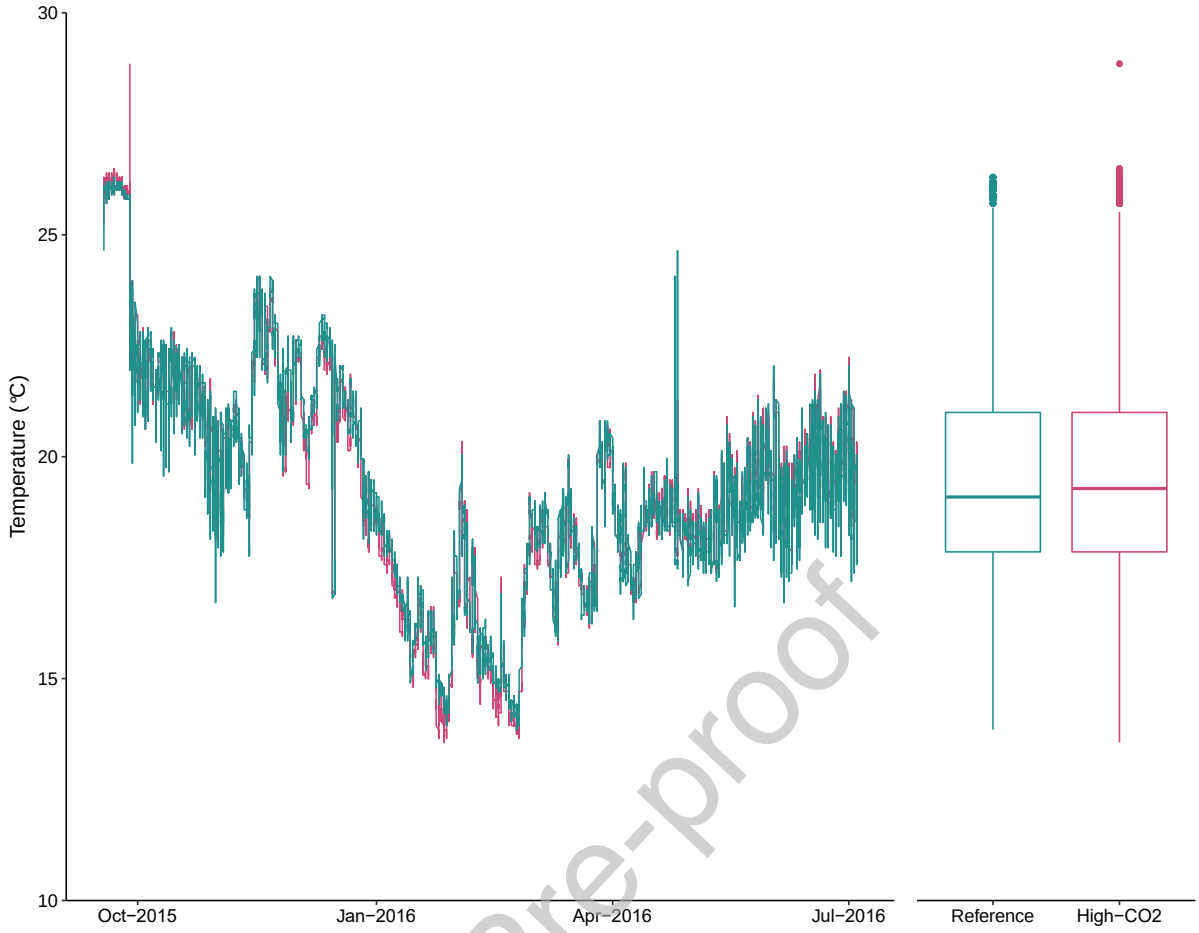

Figure S2. Temperature at reference and high CO_2 sites recorded at 15-minute intervals from boreal Autumn 2015 through boreal Summer 2016.

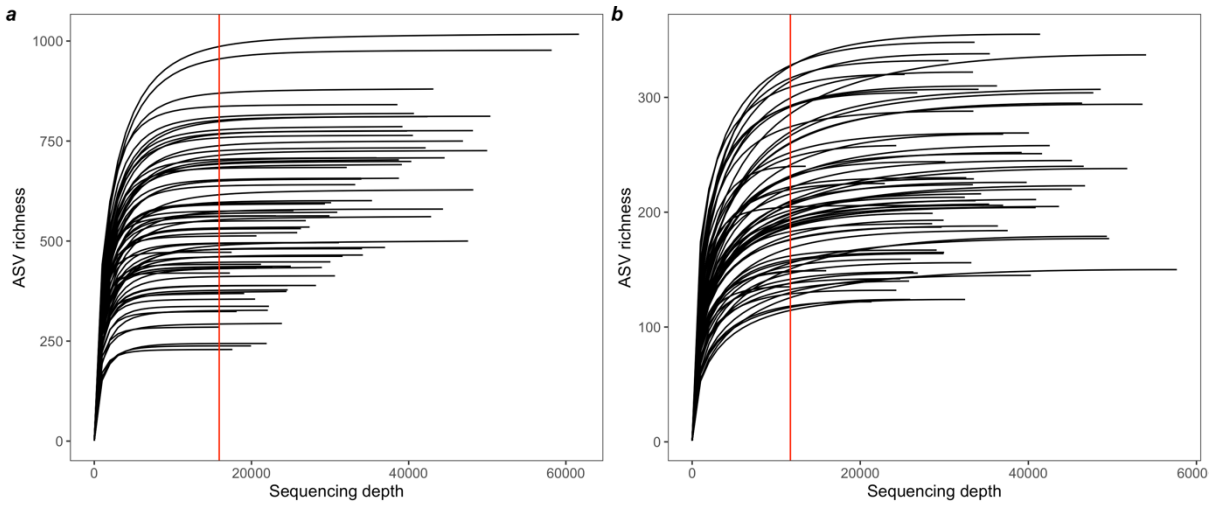

Figure S3. (a) 16S rRNA gene rarefaction curves and (b) 18S rRNA gene rarefaction curves, showing cumulative ASV richness with increasing sampling depth. Saturation of ASV richness is indicated by plateau in each rarefaction curve. Vertical red line indicates rarefaction depth for 16S rRNA gene (15,893) and 18S rRNA gene (11,689), respectively.

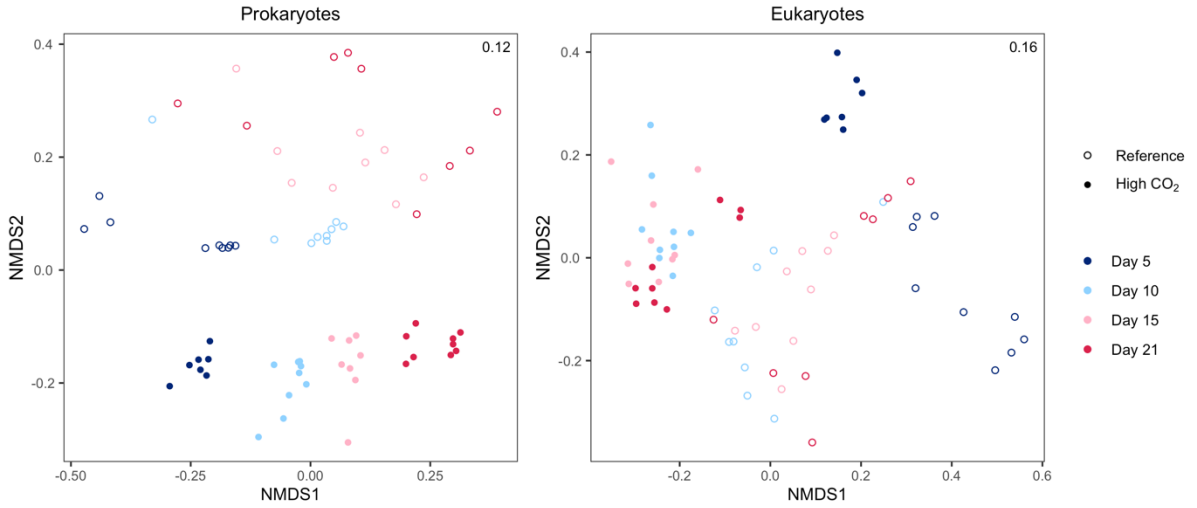

Figure S4. nMDS ordinations of prokaryotic (16S rRNA gene) and eukaryotic (18S rRNA gene) biofilm community composition under reference (open circles) and high CO_2 (filled circles) conditions at each time point, based on Bray-Curtis dissimilarity. Stress values are indicated in the upper right corner of each plot.

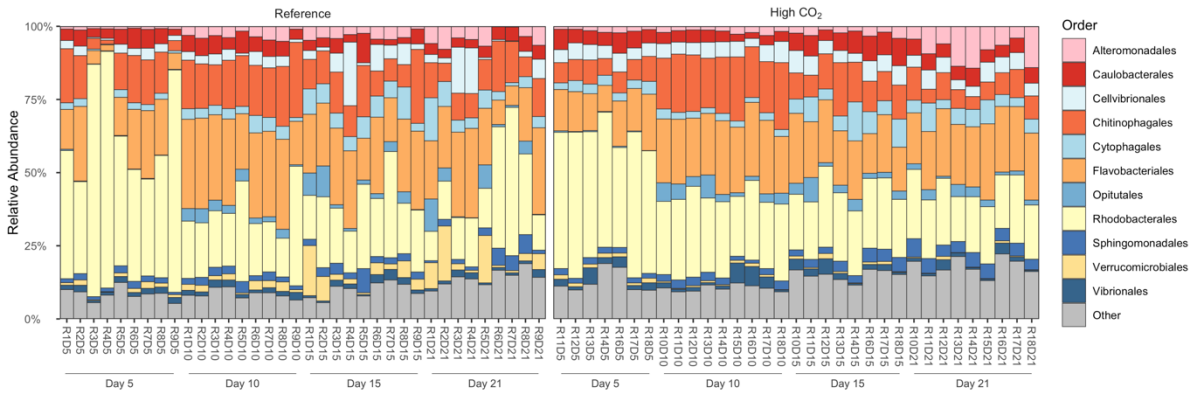

Figure S5. Order level composition of prokaryotic biofilm communities under reference and high CO_2 conditions. The 11 most abundant Orders by total read count are shown, while less abundant orders are grouped into the 'Other' category.

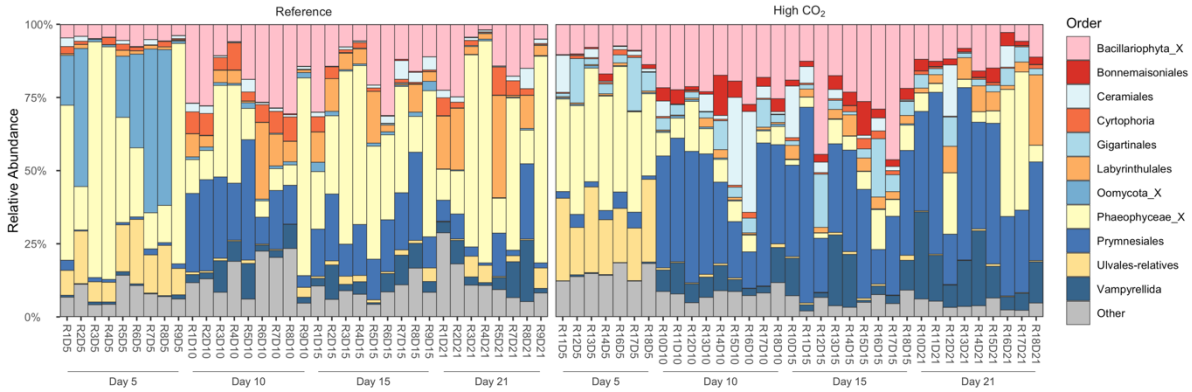

Figure S6. Order level composition of prokaryotic biofilm communities under reference and high CO_2 conditions. The 11 most abundant Orders by total read count are shown, while less abundant orders are grouped into the 'Other' category.

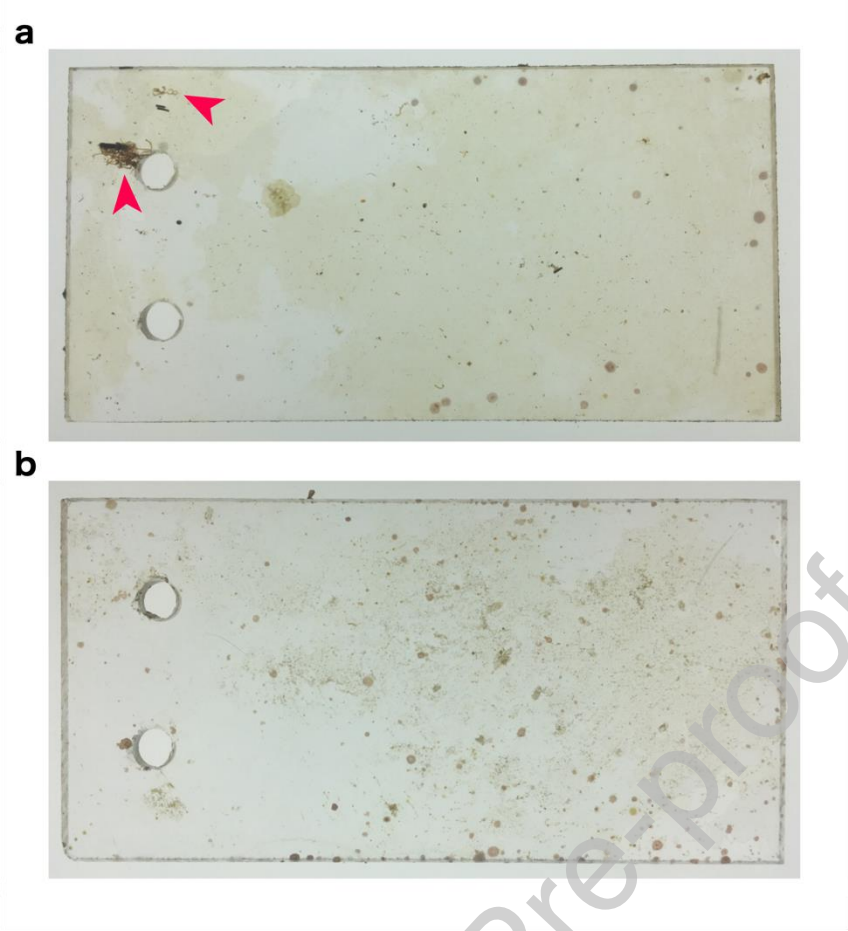

Figure S7. Representative images of colonised slides at day 21 from (a) high CO_2 and (b) reference sites. Arrows highlight colonies of the large chain-forming diatom *Biddulphia biddulphiana*.

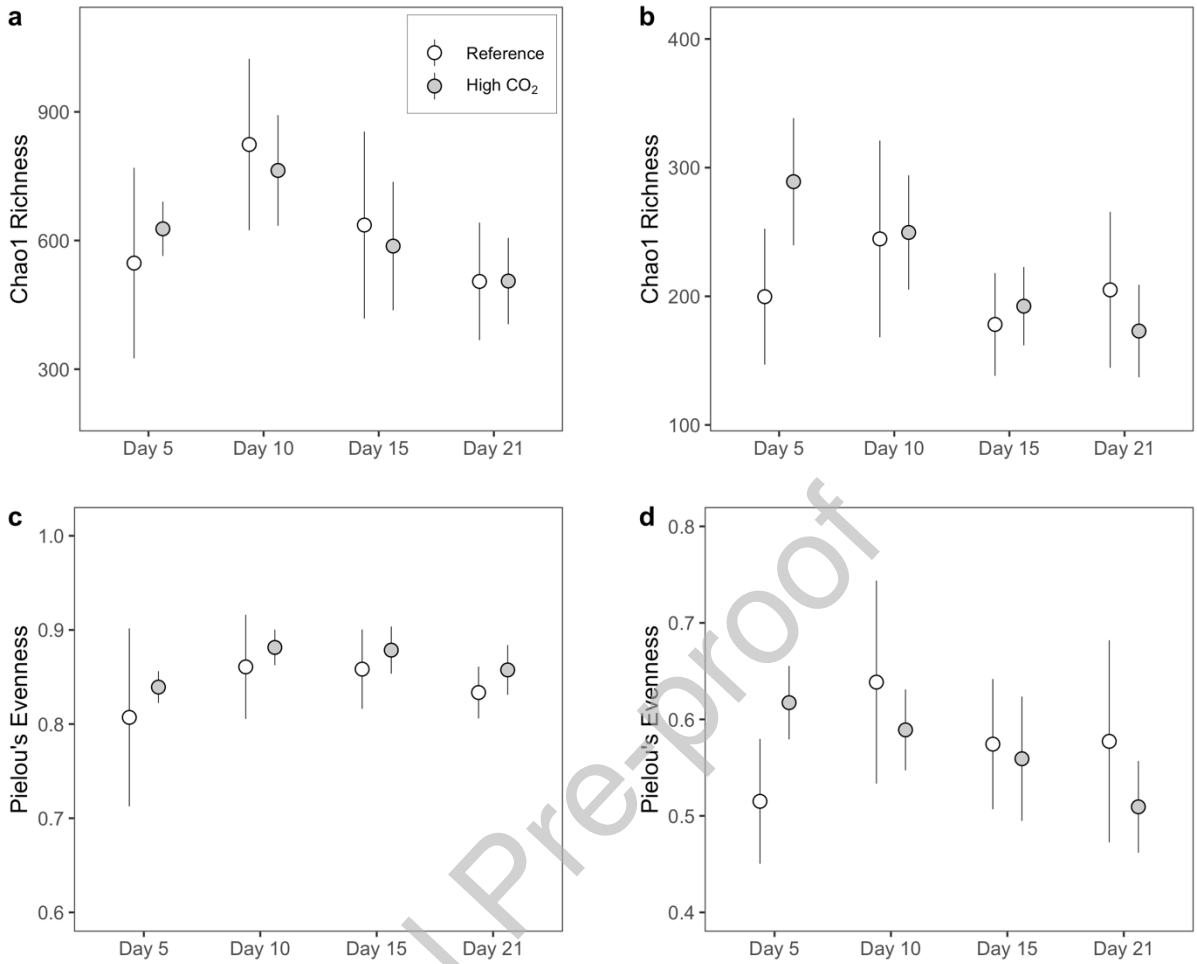

Figure S8. Chao1 richness in (a) prokaryotic and (b) eukaryotic biofilm communities, and Pielou's evenness in (c) prokaryotic and (d) eukaryotic biofilm communities under reference (n = 9) and high CO_2 (n = 9) conditions at each time point. Points represent the mean value, error bars represent the standard deviation.

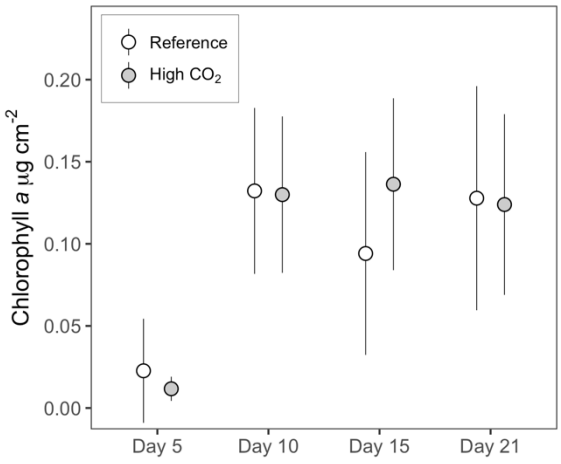

Figure S9. Concentrations of chlorophyll *a* in total biofilms colonising slides under reference (n = 9) and high CO_2 (n = 9) conditions each time point during the study. Points represent the mean value, error bars represent standard deviation.

Declaration of interests

☒ The authors declare that they have no known competing financial interests or personal relationships that could have appeared to influence the work reported in this paper.

☐The authors declare the following financial interests/personal relationships which may be considered as potential competing interests: